EES Batteries

ROYAL SOCIETY OF CHEMISTRY

REVIEW

View Article Online
View Journal | View Issue

Cite this: *EES Batteries*, 2025, **1**, 672

Electrolyte engineering promoting high-specific-energy lithium batteries in low-temperature environments

Qichao Wang, [a] Junyi Gan,[a] Yao Zhao,[a] Chenyu Yang, [a] Gongle Zhu,[b] Nana Wang, *[c] Chaofeng Zhang, [a] Jianping Yang *[d] and Tengfei Zhou *[a]

Lithium batteries have become one of the preferred power sources for various external devices due to their high energy density, mature industrial infrastructure, and diverse applications. However, the increasing demands for enhanced functionality, broader operating conditions, and increased robustness in next-generation devices highlight a critical challenge: the poor performance of lithium batteries in low-temperature environments. At low temperatures, slow lithium-ion diffusion and charge transfer dynamics, closely linked to the electrolyte, significantly hinder battery performance. The electrolyte, which facilitates ionic transport and mediates various interfacial reactions between electrodes, is pivotal in addressing these limitations. This review identifies five key factors limiting battery performance in low-temperature environments and outlines comprehensive optimization strategies to address them. These include the engineering regulation of individual electrolyte components and the compatibility coordination among various components. We thoroughly elucidate the mechanisms behind existing optimization strategies and propose future development directions and prospects for advancing low-temperature lithium battery electrolytes. By integrating rapidly evolving interdisciplinary strategies, this discussion aims to overcome the current limitations and pave the way for the next generation of high-performance lithium batteries for low-temperature environments.

Received 19th February 2025,
Accepted 19th May 2025

DOI: 10.1039/d5eb00035a

rsc.li/EESBatteries

Broader context

The modernization of electrical systems is driving an escalating demand for high-specific-energy batteries. Lithium-based systems (Li-ion/Li-metal), recognized for their high energy density and mature industrial infrastructure, dominate electrochemical energy storage. However, conventional lithium batteries operate efficiently only under moderate conditions and fail in extreme environments (*e.g.*, high plateaus, deep sea, polar regions, and space). Prolonged exposure to low temperatures causes drastic capacity loss or functional failure, primarily due to sluggish ion transport and interfacial instability. As the core components governing ion conduction and electrode–electrolyte interfacial dynamics, electrolytes are pivotal in addressing these cryogenic challenges. The key factors that limit the performance of lithium batteries in low-temperature environments, along with comprehensive optimization strategies to address these factors and the underlying mechanisms—with particular emphasis on the compatibility and coordination among various components of the electrolyte—should be thoroughly discussed.

1. Introduction

With the rapid advancement of military–civilian integration and the modernization of electrical equipment, the demand for low-temperature lithium batteries is rising, especially in extreme environments such as plateaus, deep seas, polar regions, high altitudes, and outer space (Fig. 1a). The demand for low-temperature lithium batteries is also increasing for applications in new energy vehicles, 5/6G base stations, military drones, and navigation systems.[1,2] Traditional lithium-ion batteries cannot meet the energy storage and release demands in these low-temperature environments.[3]

[a]*Institutes of Physical Science and Information Technology, Key Laboratory of Structure and Functional Regulation of Hybrid Material (Ministry of Education), Hefei 230601, China. E-mail: tengfeiz@ahu.edu.cn*
[b]*College of Chemistry, Jilin University, Changchun, Changchun, 130000, China*
[c]*Centre for Clean Energy Technology, School of Mathematical and Physical Sciences, Faculty of Science, University of Technology Sydney, Sydney, NSW, 2007 Australia. E-mail: Nana.Wang@uts.edu.au*
[d]*State Key Laboratory of Advanced Fiber Materials, College of Materials Science and Engineering, Donghua University, Shanghai 201620, China. E-mail: jianpingyang@dhu.edu.cn*

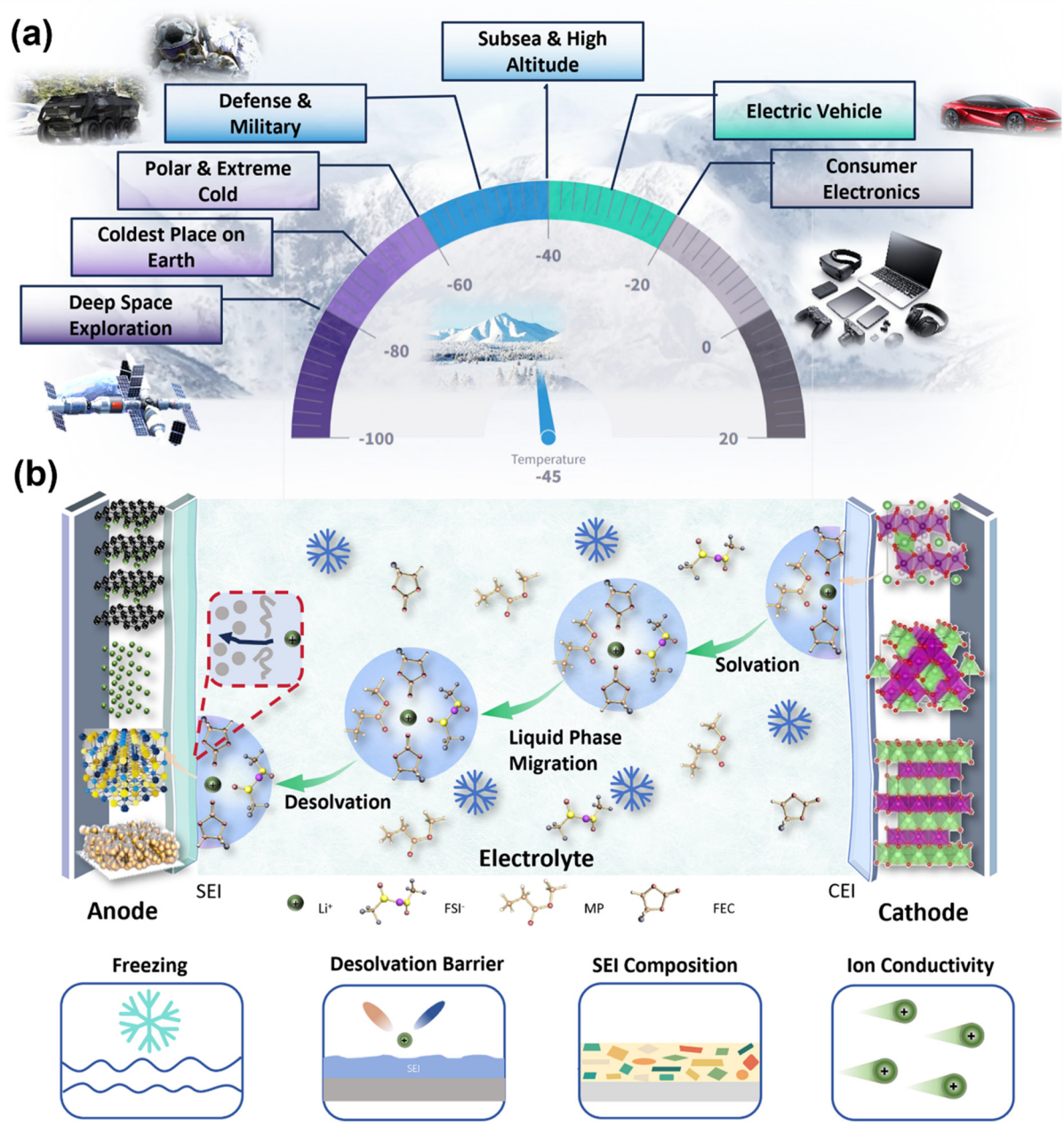

Fig. 1 (a) Potential applications of LBs in low-temperature environments. (b) Schematic representation of the discharge mechanism of LBs under low-temperature conditions.

In the military, low-temperature lithium batteries are widely used across all branches, including land, sea, air, space, and communications. These batteries are critical for various military applications, including large bases, small infantry units, aerial and space equipment, underwater devices, and unmanned combat systems. In the civilian sector, the development of the Internet of Vehicles (IoV), upgrades in consumer products, and the construction of new infrastructure have led to increased demand for low-cost, low-temperature lithium batteries for new energy transportation, logistics, and communications. In northern regions with extreme weather, such as harsh winters and high altitudes, the range of new energy vehicles is significantly reduced. Thus, the development of low-temperature lithium-ion batteries that can operate in cold environments is essential.

Temperature affects mass transport and charge transfer processes during the charging and discharging of lithium batteries. At low temperatures, the reduced kinetics of lithium ions is the primary factor limiting electrochemical performance. Fig. 1b shows the charging process of lithium batteries at low temperatures.[4–6] As shown in the figure, during charging and discharging, lithium ion migration proceeds through the following steps: (1) transport of dissolved lithium ions in the liquid phase; (2) solvation/desolvation; (3) migration at the

phase interface (including the solid electrolyte interface, SEI, and cathode/electrolyte interface, CEI); and (4) migration within the solid phase. At low temperatures, the ionic conductivity of the electrolyte decreases, hindering the solvation/desolvation of lithium ions. The migration rate of lithium ions within the electrode material and at the solid–liquid interface is significantly reduced, leading to substantial degradation in battery performance. Additionally, the anode surface becomes more susceptible to lithium plating and dendrite growth, which can cause battery failure and pose safety risks.[7,8]

The electrolyte, as a key medium bridging the anode and cathode electrodes and facilitating ion transport, significantly impacts the battery's low-temperature performance. At low temperatures, the ionic conductivity of the electrolyte decreases, charge transfer kinetics slows down, and the migration rate of lithium ions at the SEI and within the electrode decreases (Fig. 1b). These factors collectively contribute to the degradation of battery performance under cold conditions. Low temperatures also reduce the ionic conductivity of the electrolyte, increase the dissociation energy barrier, and destabilize the SEI, significantly decreasing battery capacity.[9]

To address these challenges, solvents or additives with low freezing points and viscosities, combined with lithium salts that have high dissociation efficiency, can effectively lower the dissociation energy barrier, enhance ionic conductivity, and modify the solvation structure of lithium ions, thus optimizing battery performance under cold conditions. Despite recent advances, further efforts are needed to extend the low-temperature operating range and improve battery energy density, as current results are limited to 140 W h kg^{-1} at −60 °C (Fig. 2).[10,11] This review summarizes key factors contributing to the performance degradation of high-energy batteries under low-temperature conditions, analyzes the underlying mechanisms, and discusses recent advancements in low-temperature electrolyte engineering. The article focuses on components such as lithium salts, solvents, and additives, and outlines future research directions for electrolytes in high-energy, low-temperature batteries.

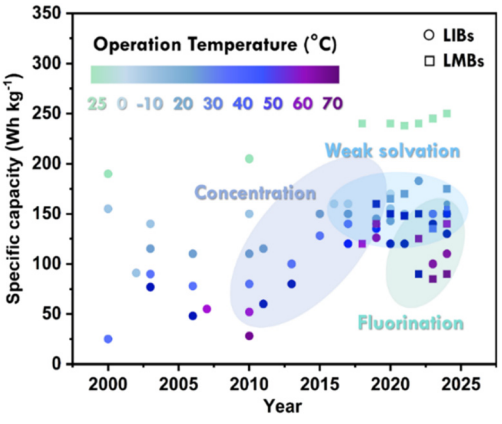

Fig. 2 Development on energy density for lithium batteries operated at low temperatures. The solid and dashed lines represent the energy density of lithium-ion batteries (LIBs) and lithium metal batteries (LMBs) from −70 °C to 25 °C, respectively.

2. Low temperature challenges

2.1 Thermodynamic and kinetic constraints on low temperature redox reactions

As shown in the Arrhenius equation, temperature is a critical factor influencing both the feasibility of a chemical reaction and its rate.

$$k = Ae^{-E_a/RT} \quad (1)$$

This equation shows that the rate of an electrochemical reaction decreases exponentially with temperature reduction, leading to considerable energy barriers within the reaction pathway. It can be inferred from these principles that the performance of batteries at low temperatures is susceptible to instability, thereby affecting the discharge specific capacity and voltage range during cycling. This poses a significant challenge for effective battery management. Within a certain temperature range, the kinetic coefficient demonstrates a strong temperature dependence. At low temperatures, ion diffusion is hindered, leading to increased electrode polarization, and the cutoff voltage is rapidly reached, reducing output capacity.[12]

The thermodynamic and kinetic properties of redox reactions at both electrodes are adversely affected by reduced temperatures, severely limiting reaction rates and lithium-ion diffusion. This bottleneck reduces the battery's capacity and energy efficiency. Engineering electrolyte additives that modulate redox kinetics at low temperatures can help alleviate these constraints, allowing for more efficient electron and ion transfer, thus improving overall cell efficiency.

2.2 Drastic decline in ionic conductivity

Temperature also significantly influences the physical and chemical properties of the electrolyte, as demonstrated by the Stokes–Einstein equation and the dielectric phenomenon:

$$D = \frac{kT}{6\pi\eta\gamma} \quad (2)$$

$$q = \frac{|Z_i Z_j| e^2}{8\pi\varepsilon\varepsilon_0 kT} \quad (3)$$

where D is the diffusion coefficient, η is the medium's viscosity, γ is the solvation radius, q is the critical distance for ion-pair formation, Z is the ion valency, ε and ε_0 are the dielectric constants of the medium and vacuum, respectively, and k is the Boltzmann constant. Furthermore, ionic conductivity, σ, is given by:

$$\sigma = \sum_i n_i \mu_i Z_i e \quad (4)$$

where n_i is the number of free ions, μ_i is the ionic mobility, and Z_i is the ion valency. Eqn (2)–(4) show that at low temperatures, increased viscosity reduces ion mobility, and solvation

shells form close ion pairs with counterions, impeding ion migration. The dielectric constant, ε, can either promote or inhibit ion dissociation, impacting the number of free ions, n_i, and thus conductivity.

At sub-zero temperatures, conventional lithium battery electrolytes exhibit a marked decline in ionic conductivity. This phenomenon is attributed to increased electrolyte viscosity and restricted ion mobility, hindering efficient lithium-ion transport across the cell. As a result, charge/discharge rates and energy output are significantly impaired.[13] Addressing this issue requires precisely engineered electrolyte formulations with low-viscosity solvents and optimized ion solvation mechanisms to sustain conductivity at low temperatures.

2.3 Formation of a high-resistance SEI

As shown in the Arrhenius equation, the kinetics of each process declines exponentially with temperature. Low temperatures promote the formation of a dense, resistive SEI layer, largely due to incomplete SEI stabilization. This resistive SEI layer inhibits lithium-ion diffusion, leading to increased interfacial impedance.[14] To mitigate this, low-temperature-compatible SEI-forming additives are essential, promoting a flexible, conductive SEI layer that can enhance ion permeability and minimize impedance under harsh conditions.

2.4 Electrolyte crystallization and phase instability

Conventional organic solvents in liquid electrolytes are prone to crystallization or phase separation at low temperatures, disrupting the continuity of the ion transport pathways. Such phase instability not only compromises ionic conductivity but also increases internal cell resistance. Developing supercooled or low-melting-point solvents can stabilize electrolyte phases, thereby preventing phase separation and maintaining electrochemical performance in cold environments.

2.5 Enhanced lithium plating and dendrite formation risks

The morphology of lithium deposition varies with temperature, influenced by distinct nucleation and SEI characteristics of lithium metal anodes. For example, the SEI formed below −80 °C in DOL/DME electrolytes is thinner and more chemically stable than the SEI formed at room temperature. However, the SEI's ionic conductivity decreases at −30 °C, with low-temperature-induced structural changes increasing resistance and limiting Li^+ diffusion, significantly impacting battery performance.[15]

At low temperatures, lithium-ion diffusion is drastically reduced, leading to lithium plating on the anode surface due to limited ion availability and reaction kinetics. This phenomenon risks forming dendrites that can cause internal short circuits, posing severe safety hazards. Designing electrolytes with anti-plating additives and ion-dispersing properties is essential for mitigating lithium dendrite formation and ensuring the stable and safe operation of lithium batteries under low-temperature conditions.

3. Electrolyte engineering to improve low-temperature performance of LBs

3.1 Modifying lithium salts to enhance electrolyte properties

The performance of the electrolyte is significantly influenced by the presence of lithium salts, which affect the dissociation, solubility, and ionic conductivity of the SEI. Additionally, lithium salts can also reduce the freezing point of the electrolyte *via* solvent colligative effects.

3.1.1 $LiPF_6$ enhances thermal stability and overall performance. $LiPF_6$ demonstrates high dissociation, leading to the production of LiF and the formation of a LiF-rich inorganic SEI.[16,17] It exhibits minimal corrosion towards aluminum and possesses other favorable properties, making it the most widely used salt in non-aqueous electrolytes. Cho *et al.*[18] reported a low-temperature electrolyte with methyl propionate (MP) as the solvent. This $LiPF_6$/MP/FEC electrolyte enabled the battery to successfully cycle for 100 cycles at a rate of 0.2C at −20 °C without capacity attenuation. Fig. 3a illustrates the ionic conductivities of three electrolytes at different temperatures, the M9F1 electrolyte exhibiting the highest ionic conductivity over an extensive temperature range. Moreover, the full cell employing this electrolyte is capable of maintaining 60% of the room temperature capacity (RTC) at −40 °C. However, it is sensitive to moisture and reacts with H_2O to generate HF, which can corrode electrodes and reduce battery capacity, limiting its low-temperature application. Consequently, researchers have synthesized various lithium salts to improve low-temperature performance.

3.1.2 Borates ($LiBF_4$, LiBOB, and LiDFOB) reduce charge transfer resistance. $LiBF_4$, LiBOB, and LiDFOB have been utilized as alternatives to $LiPF_6$ in low-temperature electrolytes. $LiBF_4$-based electrolytes showed lower RCT compared to $LiPF_6$-based electrolytes and demonstrated superior capacity retention at −30 °C. However, the poor ionic conductivity and severe side reactions with the lithium anode led to an unstable SEI. LiBOB has excellent film-forming ability and functions effectively below zero, but its high viscosity limits its low-temperature application. LiDFOB integrates the advantageous properties of LiBOB and $LiBF_4$, rendering it more appropriate for applications in low-temperature electrolytes (Fig. 3b).[19] Han *et al.*[22] proposed a new electrolyte (2.4 M LiDFOB/EA/FEC) that solved Li^+ transport dynamics and stabilized the interface at low temperatures. The $LiNi_{0.9}Co_{0.05}Mn_{0.05}O_2$ (NCM90)||Li full cell exhibited discharge capacities of 173 mA h g^{-1} at −40 °C and 152 mA h g^{-1} at −60 °C with this electrolyte. Additionally, LiDFOB is commonly utilized in binary or ternary salt systems to decrease interface resistance, expand the variety of anions, and improve low-temperature performance (Fig. 3c). Liang *et al.*[21] reported that ternary BF_4^-, PF_6^- and difluoro (oxalato) borate anions could form complexes in tetrahydrofuran (THF), enhancing the electrochemical stability of the solvent and broadening the electrochemical window (2.7–4.5V). The formulated electrolyte achieved 93.4% capacity retention after 100 cycles at −30 °C and 0.05C.

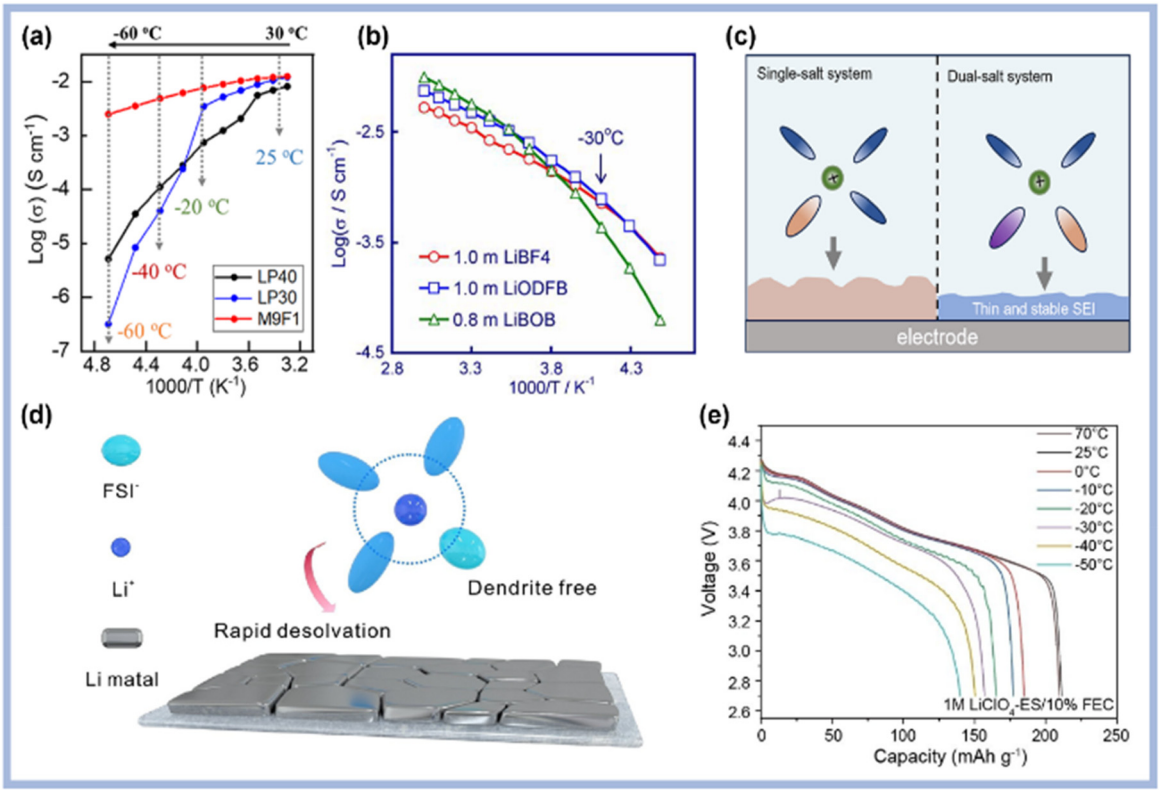

Fig. 3 (a) Ionic conductivities of different electrolytes measured at various temperatures. Reproduced from ref. 18. Copyright 2021, American Chemical Society. (b) Ionic conductivity of 1.0 M Li BF_4, 1.0 M LiODFB, and 0.8 M LiBOB in PC/EC/EMC (1 : 1 : 3 by wt). Reproduced from ref. 19. Copyright 2022, Elsevier. (c) Schematic of the mechanism of dual-salt. (d) Schematic diagram of the relationship between Li deposition morphology and solvating power of the solvent at low temperature. Reproduced from ref. 20. Copyright 2022, Wiley-VCH. (e) Cycling performance of NCM811|| Li cells with 1 M $LiClO_4$-ES/10% FEC at different temperatures. Reproduced from ref. 21. Copyright 2024, Wiley-VCH.

3.1.3. Sulfonylimides (LiFSI and LiTFSI) improve ionic conductivity. LiFSI possesses high solubility, excellent conductivity, and fast desolvation kinetics, which enables its extensive application in low-temperature electrolytes. Jin *et al.*[23] designed an electrolyte containing 1 M LiFSI in DOL/DME, noting that low-affinity solvents facilitate fast desolvation. The Li||NCM523 cells with this electrolyte retained 66% capacity at −40 °C compared to room temperature. However, LiFSI poses environmental risks and high preparation costs. LiTFSI-based electrolytes, with higher ionic conductivity and improved interfacial stability, have garnered attention. Ma *et al.* reported an ether-based electrolyte containing 1 M LiTFSI in dimethoxymethane (DMM), which showed better coordination between Li-ions and anions, lower desolvation energy, and favorable SEI formation (Fig. 3d). The Li||SPAN full cell demonstrated stable cycling for 500 cycles and maintained an average CE of 97.67% at −20 °C. At −40 °C, the cell exhibited an initial discharge capacity of 422.3 mA h g^{-1} and retained 63.8% capacity after 120 cycles at 0.1C.[20] Nevertheless, the anion of LiTFSI can corrode aluminum current collectors under high voltage, compromising the cycling stability and safety of batteries. Additionally, the mechanism by which $TFSI^-$ forms the CEI remains unclear. These limitations underscore the need to develop novel sulfonimide salts for advanced electrolyte systems.

3.1.4. Asymmetric salt ($LiClO_4$) lowers the freezing point. The structure of lithium salts also impacts electrolyte performance. Wang *et al.* investigated the influence of asymmetric lithium salts (lithium perchlorate ($LiClO_4$)) in an ES/10% FEC electrolyte, and discovered that augmenting the asymmetric structure would reduce the freezing point.[21] The ES/FEC electrolyte remained liquid at −40 °C. Using this optimized electrolyte, the NCM811||Li full pouch cell demonstrated 83.3% of RTC at −20 °C (Fig. 3e).

3.2. Modifying the solvent to improve Li^+-solvent interactions

The solvent is a critical component of low-temperature electrolytes, and its design aims to reduce viscosity and freezing point, enhance ionic conductivity, and modify the solvation structure to accelerate the kinetics of desolvation. Solvents can be categorized as follows.

3.2.1 Conventional solvents

Carbonate-based solvents for lowering freezing points. Carbonate-based solvents are frequently combined with other solvent types to form binary co-solvent systems, which exhibit significantly lower melting points compared to their individual components. Ai *et al.*[24] found that co-solvents with low melting points effectively broaden the operational temperature range of the electrolyte (Fig. 4a). Carbonates can also form quaternary

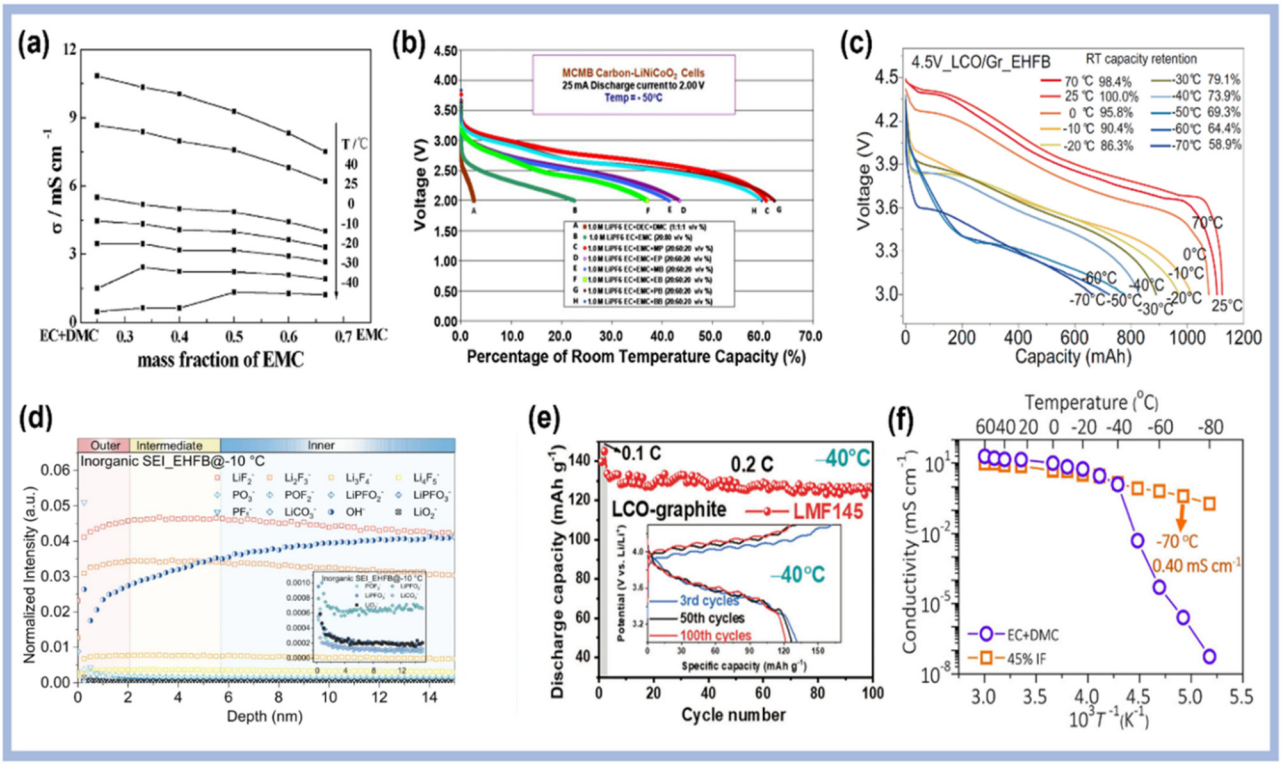

Fig. 4 (a) Ionic conductivity of 1 M $LiPF_6$ in EC/DMC/EMC with different EMC ratios at various temperatures. Reproduced from ref. 24. Copyright 2004, Elsevier. (b) Discharge capacity of carbon–$LiNiCoO_2$ cells at −50 °C and C/16 using 1.0 M $LiPF_6$ in EC/EMC/X (20 : 60 : 20 vol%) (where X = MP, EP MB, EB, PB, and BB). Reproduced from ref. 27. Copyright 2010, Institute of Physics Publishing. (c) RT charge–LT discharge protocol. Reproduced from ref. 29. Copyright 2023, Springer Nature. (d) TOF-SIMS depth profiles of inorganic SEI functional groups after prolonged cycling (EHFB electrolyte, −10 °C). Reproduced from ref. 29. Copyright 2023, Springer Nature. (e) Cycling stabilities of the LCO||graphite full cell in LMF145 at −60 °C and 0.05C. Reproduced from ref. 30. Copyright 2023, Wiley-VCH. (f) Ionic conductivities of different electrolytes at various temperatures. Reproduced from ref. 31. Copyright 2023, Royal Society of Chemistry.

multicomponent systems when combined with other solvents.[25,26] Smart *et al.*[27] investigated diverse esters, such as methyl propionate (MP), ethyl propionate (EP), and methyl butyrate (MB), as constituents of the electrolyte (Fig. 4b). The electrolyte containing MP exhibits excellent capacity at 0.1C and −50°/−60 °C. Another electrolyte composed of ethyl acetate (EA) exhibits an ionic conductivity of 1.7 mS cm^{-1} at −40 °C and enables the full cell to retain 90% of RTC.[28] Chen *et al.*[29] investigated the effects of ethyl acetate-based solvents with different degrees of fluorination and fluorine substitution sites. They measured the discharge capacity of the battery at different temperatures and analyzed the composition of the SEI after long-term cycling under low-temperature conditions using TOF-SIMS (Fig. 4c and d). The electrolyte exhibits a conductivity of 1.46 mS cm^{-1} at −90 °C and enables pouch cells to maintain 98% of their initial capacity after 200 cycles at −10 °C and 0.1C.

Ester-based solvents to facilitate ion migration. Compared to carbonates, low-molecular-weight esters exhibit lower melting points, viscosities, and higher dielectric constants. These properties enable esters to serve as efficient electrolyte solvents, promoting rapid Li^+ ion transport at low temperatures.[32] Initially, esters were used as co-solvents in EC and PC-based electrolytes. Li *et al.*[33] developed an EA-based electrolyte by combining high-concentration electrolytes (HCE) and additive strategies. The low freezing point of EA stabilizes Li^+ transport at low temperatures, while the high concentration of $LiPF_6$ and FEC ensures the formation of a LiF-rich inorganic SEI and suppresses side reactions between EA and Li. Methyl propionate, which has a molecular weight similar to ethyl acetate, also demonstrates excellent low-temperature performance.[34]

Additionally, the introduction of a diluent to the ester-based electrolyte to form a low-temperature high-concentration electrolyte (LHCE) can further enhance electrolyte performance. Lei *et al.*[30] found that the presence of fluorobenzene (FB) promotes anion entry into the solvation shell through dipole–dipole interactions and increases the proportion of stable free solvent molecules. With the diluent, methyl acetate (MA) can act as the sole electrolyte solvent to improve ultra-low temperature performance in LIBs (Fig. 4e). Liu *et al.* introduced isobutyl formate (IF) as an anti-freezing agent in DMS-based electrolytes, the ionic conductivity of the electrolyte containing 45% IF shows a slower decline at low temperatures (Fig. 4f).[31]

Ether-based solvents to reduce viscosity and improve anode compatibility. Compared with carbonates, ethers possess ultra-low freezing points, excellent compatibility with lithium metal, and rapid Li^+ transport kinetics.[35] These advantages have

made ethers a preferred choice for low-temperature electrolytes. However, ethers are susceptible to oxidation and decomposition at high potentials, which limits their application range.[36,37] Holoubek *et al.* selected diethyl ether (DEE) as the sole solvent for LIBs (Fig. 5a).[38] They proposed that the solvation structure of the electrolyte governs charge-transfer behavior at low temperatures, owing to the weak solvation nature of the solvent. A similar effect was observed with dimethyl ether (DME) as the solvent.[39] The addition of dibutyl ether (DBE) significantly enhanced the low-temperature performance of Li–S cells due to its weak Li^+ solvent-binding interactions, promoting a highly ion-paired solvation structure at low salt concentrations.[40] The backbone structure of ethers also influences their oxidation stability. Chen *et al.*[41] investigated the correlation between the ion-solvent coordination extent in the electrolyte and the electrochemical behavior through comparing ethers featuring distinct $-(CH_2)_n-$ chain lengths, such as DME and 1,3-dimethoxypropane (DMP). They found that DMP, featuring a five-membered chelating ring, can form a more stable six-membered chelate complex with Li^+, thereby significantly enhancing Li^+ solvation and effectively reducing side reactions with labile free solvent molecules (Fig. 5b).

Yoon *et al.* developed a ternary solvent low-temperature electrolyte based on ether/hydrofluoroether and fluoroethylene carbonate (FEC).[44] Compared to other ethers, tetrahydrofuran (THF) has a more symmetric structure, reducing the electron density of the oxygen atom and enhancing solubility for $LiNO_3$, which has garnered significant attention. The electrolyte composed of LiFSI–$LiNO_3$/THF maintained a high conductivity of 2.87 mS cm^{-1} at −60 °C. Liang *et al.*[42] proposed a THF-based ternary-anion electrolyte to improve electrolyte kinetics at low temperatures. They found that the interaction between the three anions was weakened by repulsive forces, leading to predominant coordination of Li^+–NO_3^- in the Li^+ solvation structure (Fig. 5c). At −60 °C, the optimized electrolyte exhibited a high ionic conductivity of 3.39 mS cm^{-1}. In a binary ether-based electrolyte (1 M LiFSI in MTHF/THF, containing 1 wt% $LiNO_3$), the Li||$CoSeO_x$ cell demonstrated superior low-temperature performance.[43] The weak Li^+-solvating MTHF reduced the kinetic barrier for Li^+ desolvation, while THF, with a high donor number, enhanced the solubility of $LiNO_3$, resulting in high ionic conductivity while maintaining weak Li^+-solvation effects. FTIR analysis revealed the presence of solvent-derived C–C bonds and FSI-derived N–S bonds within the SEI (Fig. 5d).

Naoi *et al.*[45] proposed non-flammable hydrofluoroether as a solvent for low-temperature applications. The branched hydrofluoroether 2-trifluoromethyl-3-methoxyperfluoropentane (TMMP) can be incorporated into the carbonate-based electrolyte, reducing the melting point of the electrolyte and concurrently generating a low-surface-energy SEI to enhance the transport rate of lithium ions at low temperatures. At −20 °C,

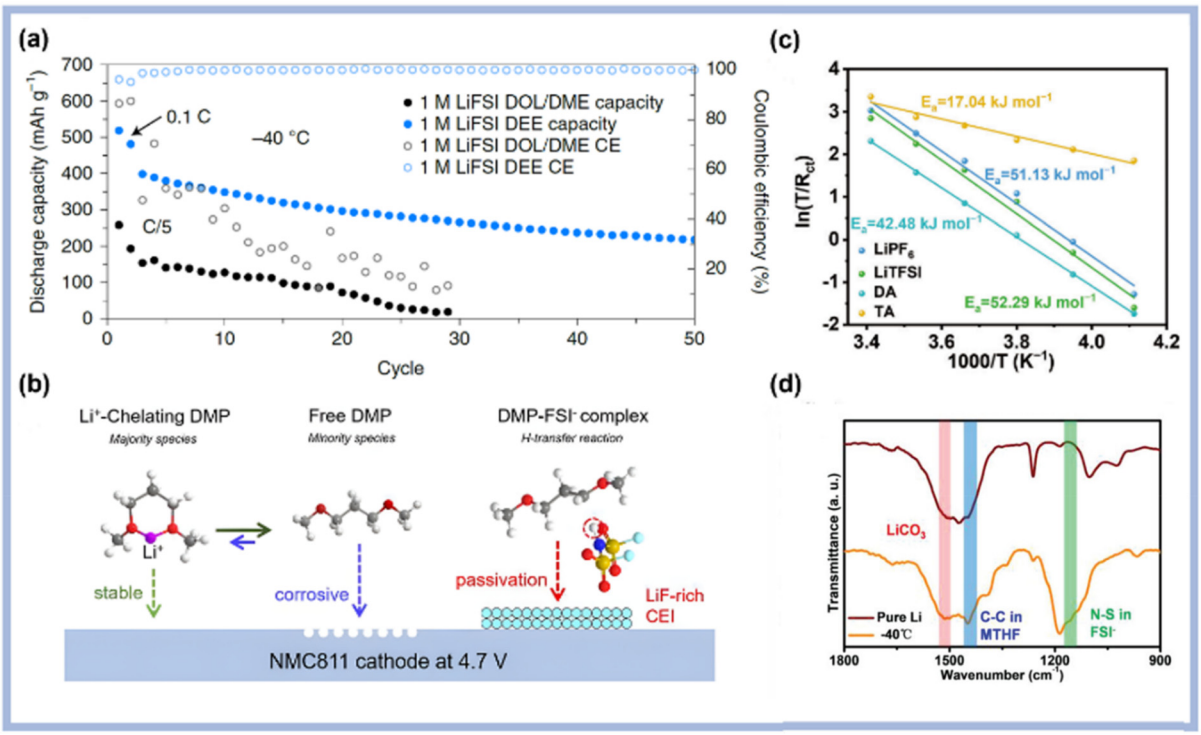

Fig. 5 (a) Cycling performance using different electrolytes at −60 °C and 0.2C. Reproduced from ref. 38. Copyright 2021, Springer Nature. (b) Electrolyte species and their roles at the cathode surface. Reproduced from ref. 41. Copyright 2023, Wiley-VCH. (c) The activation energies of R_{ct} fitted by the Arrhenius equation from 20 to −30 °C for different electrolytes. Reproduced from ref. 42. Copyright 2024, Wiley-VCH. (d) FTIR spectra of Li metal anodes before and after 10 cycles at −40 °C. Reproduced from ref. 43. Copyright 2022, Wiley-VCH.

the electrolyte containing TMMP enables the capacity of the MCMB||LCO battery to remain 60% of RTC, approximately 20% higher than that of the base electrolyte. However, ether-based solvents suffer from poor oxidative stability and tend to decompose under high-voltage conditions, resulting in irreversible capacity loss and degraded cycling performance. These limitations necessitate the development of multi-component solvent systems or novel electrolyte formulations to address these challenges.

Nitrile-based solvents to lower solvation energy. Researchers have also explored organic solvents containing sulfur (S), nitrogen (N), or phosphorus (P) for low-temperature electrolytes.[46,47] Nitrogen-containing solvents, in particular, have garnered attention for their ability to reduce interfacial impedance and facilitate the formation of a highly efficient solid electrolyte interphase (SEI) layer, making nitrides a promising candidate for low-temperature applications.[48]

In contrast to carboxylic acid esters and ether solvents, nitriles exhibit higher molecular polarity and dielectric constants, which makes them a distinctive type of electrolyte co-solvent for LBs. Luo *et al.*[49] prepared an electrolyte with isobutyronitrile (iBN) as a co-solvent. The resulting electrolyte, consisting of 8.33 vol% ethylene carbonate (EC), 31.67 vol% ethyl methyl carbonate (EMC), and 60 vol% iBN, demonstrated a sufficiently high conductivity of 1.152 mS cm^{-1} at −70 °C. The adiponitrile (ADN)-based electrolyte consisting of LiFSI and LiODFB in ADN/EC could expand the operational temperature window.[50] Lu *et al.* found that the use of fluoroacetonitrile (FAN) enabled the formation of a small solvation sheath, which facilitated fast solvation and desolvation processes.[51] The FAN-based electrolyte exhibited a high ionic conductivity of 11.9 mS cm^{-1} at −70 °C. While nitrile-based electrolytes exhibit excellent low-temperature performance, they still face critical challenges such as poor reductive stability, severe interfacial side reactions, high toxicity, elevated production costs, and significant environmental risks, all of which demand urgent resolution.

3.2.2 Fluorinated solvents. The addition of fluorinated solvents to electrolytes is a widely used strategy to enhance battery performance. Fluorination can reduce the electron density around the oxygen atom in the solvent, facilitating the desolvation process during electrochemical reactions. It can also decrease the surface tension of solvent molecules, improving electrolyte wettability and reducing contact resistance. Additionally, incorporating fluorinated solvents can enhance interfacial chemistries, promoting faster ion transport at lower temperatures.[52,53]

Fluoride ester-based solvents to improve interface compatibility and enhance the desolvation rate. Research has shown that fluorinated carboxylic acid esters can enhance the low-temperature performance of electrolytes.[54] The addition of methyl difluoroacetate (MDFA) and ethoxy-pentafluoro-cyclotriphosphazene (PFPN) optimizes the solvation–coordination environment, thereby accelerating desolvation kinetics. Yang *et al.* examined the evolution of the SEI at various temperatures using an electrolyte containing a weakly solvated molecule, ethyl trifluoroacetate (ETFA).[55] Electrolytes containing MDFA, PFPN, and fluoroethylene carbonate (FEC) maintain high capacity at −50 °C, while those containing ETFA achieve high reversible capacity at −30 °C. Furthermore, LiFSI electrolytes in pure ETFA exhibit a wide electrochemical window and low solvation energy.

Fluorinated esters can also be incorporated as co-solvents into traditional carbonate electrolytes to enhance lithium salt solubility, regulate the solvation structure, and stabilize the interface.[56] Cui *et al.*[57] introduced monofluorinated ester (MTFA) into a $LiPF_6$–dimethyl carbonate–fluoroethylene carbonate system. The resulting electrolyte enabled a 1 A h cell to maintain 0.65 A h at a 2C discharge rate and showed virtually no capacity fade at 0.2C after 80 cycles at −20 °C. Mo *et al.*[58] explored the influence of the fluorination degree on electrolyte performance; they found that ethyl difluoroacetate (EDFA), with a moderate degree of fluorination, exhibited better salt dissociation and a more balanced solvation structure compared to highly fluorinated solvents. The EDFA-FEC electrolyte facilitates rapid desolvation and high ionic conductivity, and promotes the fast diffusion of Li^+ in the SEI, providing excellent low-temperature performance (Fig. 6a). Wang *et al.*[59] investigated the influence of different degrees of fluorination in ethylene carbonate derivatives on the Li^+ solvation shell. They found that the degree of fluorination affected ion-dipole interactions, with DFEC demonstrating faster ion desolvation behavior compared to non-fluorinated solvents like EC (Fig. 6b). Xu *et al.*[60] designed a 1 M LiFSI electrolyte in a mixture of MDFA and MDFSA, which enabled the full cell to retain 93.9% of its capacity after 260 cycles at −30 °C and 0.1C, with an average coulombic efficiency (CE) of 99.98% (Fig. 6c). Xiao *et al.*[61] developed a fluorinated carbonate electrolyte using bis(2,2,2-trifluoroethyl) carbonate (BTC) as the solvent (Fig. 6d). The fluorination of the solvents improved anodic stability at high voltages and accelerated Li^+ desolvation, resulting in excellent electrochemical kinetics.

Fluoride ether-based solvents to regulate the solvation structure and broaden the electrochemical window. Fluorinated ethers, due to their enhanced antioxidation properties and improved interface compatibility, have been explored for electrolyte applications.[62,63] Zhang *et al.*[64] synthesized monofluorinated bis(2-fluoroethyl) ethers (BFE) as solvents to dissolve LiFSI. The resulting electrolyte possesses high ionic conductivity and a wide electrochemical window, and enhances the cycling stability of the battery. The monofluoro substitution maximized ion conductivity by optimizing the coordination interaction between fluorine atoms and Li^+ cations (Fig. 6e). The Li||NCM811 coin cell with this BFE electrolyte showed excellent cycling stability, retaining up to 80% capacity after 300 cycles at 3.5 and 7 mA cm^{-2} at 25 °C. Even at −30 °C, the cell maintained over 90% capacity after 150 cycles at 1.75 mA cm^{-2}. As shown in Fig. 6f, the BFE electrolyte exhibits more uniform and dense lithium deposition. Bis(2-fluoroethoxy) methane (BFME) is a monofluorinated straight-chain ether. The fluorine substitution at the β-C position significantly enhances the solvation capability of the electrolyte, thereby improving its overall performance in electrochemical appli-

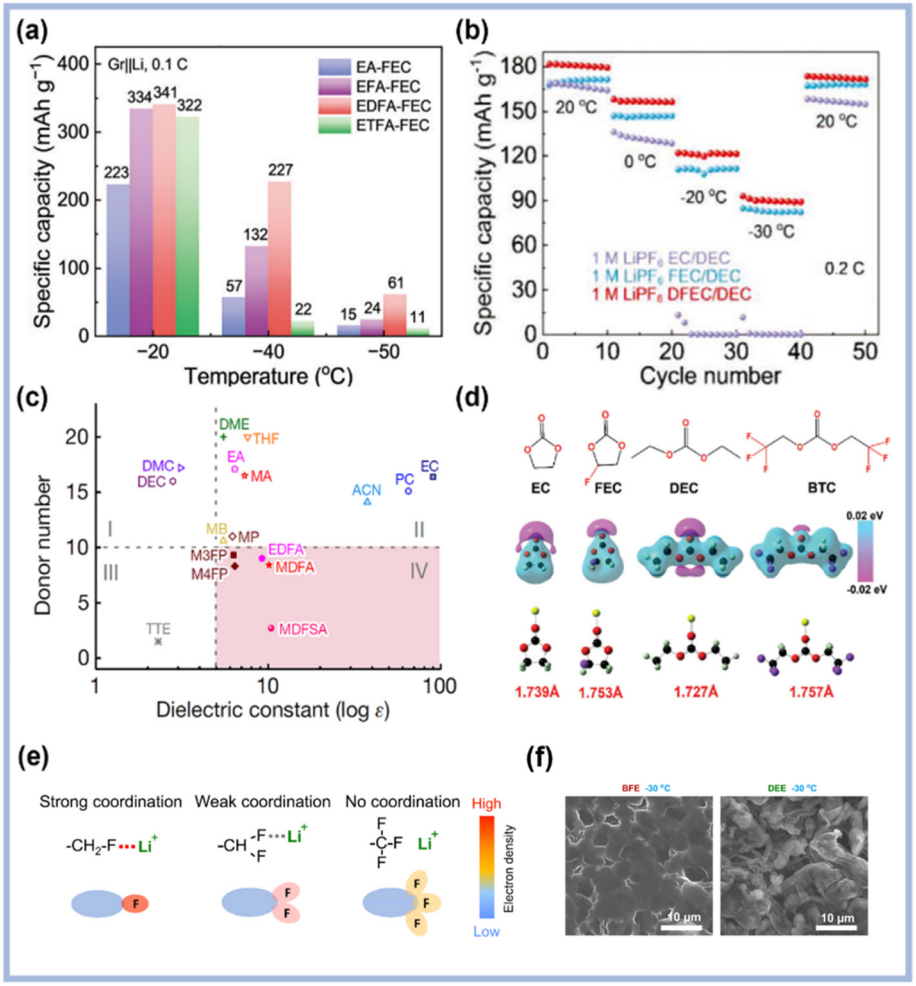

Fig. 6 (a) Discharge capabilities of pouch cells with EDFA-FEC and EA-FEC at 0.2C at different temperatures after fully charging at 25 °C. Reproduced from ref. 58. Copyright 2023, Wiley-VCH. (b) Rate performance of NCM811||Li cells at 0.2C from 20 to −30 °C. Reproduced from ref. 59. Copyright 2021, Wiley-VCH. (c) The solvent diagram of DN *versus* dielectric constant. Reproduced from ref. 60. Copyright 2023, Springer Nature. (d) Molecular structure, charge distribution and optimised structure of liquid solvents. Reproduced from ref. 61. Copyright 2023, Elsevier. (e) The coordination chemistry of monofluoride, difluoro, and trifluoro groups. Reproduced from ref. 62. Copyright 2023, Springer Nature. (f) SEM images of plated Li on Cu foil in BFE and DEE electrolytes at −30 °C, respectively. Reproduced from ref. 62. Copyright 2023, Springer Nature.

cations.[65] Fluoride ethers can also be employed as diluents in LHCEs, which do not participate in the solvation structure of Li^+.[66] Jiang *et al.* developed a fluorinated ether, bis(2,2,2-trifluoroethyl) ether (BTFE).[67] The resulting cells delivered 90 mA h g^{-1} at 0.1C at −20 °C. Although fluorinated solvents facilitate desolvation processes, they exhibit drawbacks including low ionic conductivity, high viscosity, toxicity, and high costs. Therefore, combining them with other solvents is necessary to tailor electrolyte properties.

3.3 Employing additives to regulate the multiple interfaces of RLBs

By adding small amounts of specific additives, the high-voltage stability, film-forming ability, and desolvation energy of the electrolyte can be improved, thus boosting its low-temperature performance. Additives can generally be classified as follows.

3.3.1 N-containing additives to suppress lithium dendrite growth. Lithium nitrate ($LiNO_3$), due to its higher redox potential compared to other anions or solvents, is preferentially reduced on the lithium surface, forming a robust SEI enriched with Li_3N and Li_2O inorganic components. Li_3N exhibits a relatively high ionic conductivity, and coupled with organic components, forms a SEI with outstanding mechanical properties to endure the volume changes, while facilitating ion transport.[68,69] However, the poor solubility of $LiNO_3$ in carbonates and esters limits its widespread use. To address this, various methods have been employed to enhance its solubility in electrolytes, thereby improving low-temperature battery performance.

Increasing the solubility of $LiNO_3$. Xu *et al.*[70] introduced a synergistic additive, triglyme (G3)-$LiNO_3$ (GLN), into a carbonate-based electrolyte to form a SEI with uniform Li-ion flux, enabling dendrite-free and reversible lithium plating.

Moreover, the introduction of tris(pyrrolidinophosphine) oxide (TPPO), a high DN solvent, facilitated the dissolution of $LiNO_3$ in the carbonate electrolyte, further enhancing the low-temperature performance of the cells. TPPO's high DN allows $LiNO_3$ to dissolve more easily in the electrolyte, promoting the formation of a Li_3N-rich SEI film (Fig. 7b).[71] Similarly, Chen *et al.*[72] used DMSO, a high-donor-number solvent (HDNS), to dissolve $LiNO_3$ and added PC, a low-donor-number solvent (LDNS), to improve the electrolyte oxidative stability. Jiang *et al.*[73] reported that combining $LiNO_3$ with vinylene carbonate (VC) in an ether-based electrolyte improved the electrochemical behavior over a wide temperature range. The synergistic effects of $LiNO_3$ and VC, which decompose on the electrode surface upon entering the electrolyte solvation shell, resulted in the formation of a stable bilayer SEI.[74] Qiu *et al.*[75] explored the mechanisms behind concentrated salt electrolytes, using LiFSI–$LiNO_3$–LiFSI ternary salts in a THF solvent. The combination of $LiNO_3$ and LiFSI helped form stable Li_2O–LiF-rich SEI layers, while LiFSI stabilized the electrolyte at high concentrations. Additionally, sulfolane (SL) demonstrated similar capabilities in dissolving $LiNO_3$, thereby enhancing electrochemical performance.[76]

Other additives beyond $LiNO_3$. Isosorbide dinitrate (ISDN), a nitrate compound, can also be used as a substitute for $LiNO_3$. Zhang *et al.*[81] blended ISDN into 1 M LiFSI in DME/HFE, improving the cycle life of high-voltage batteries. The decomposition products of ISDN, including LiN_xO_y, are identified as the key components for enhancing the uniformity of

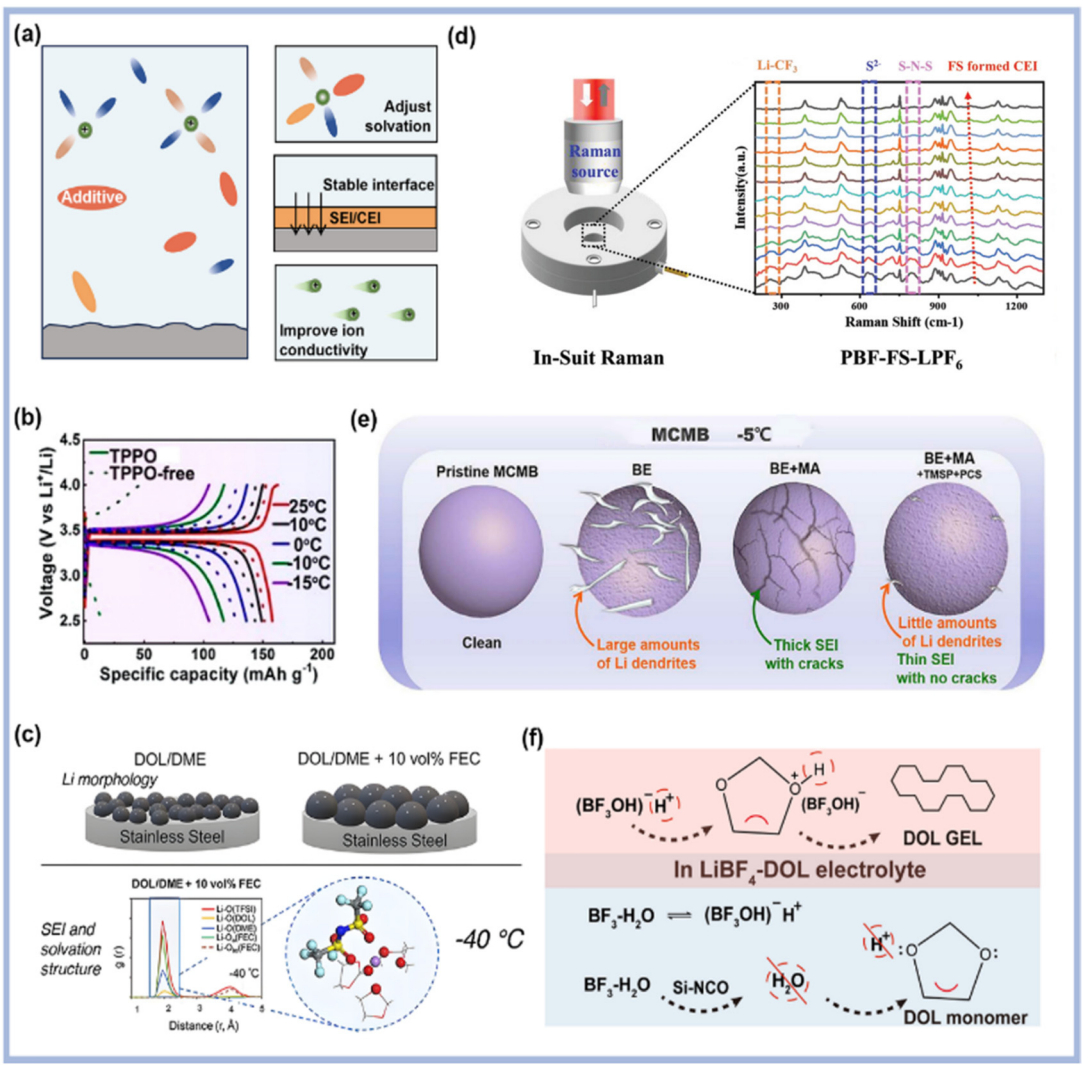

Fig. 7 (a) Effects of additives on improving the performance of the cell at low temperature. (b) The charge–discharge curves using different electrolytes. Reproduced from ref. 70. Copyright 2021, American Chemical Society. (c) Schematic illustration of the effects of the FEC additive on interfaces of the cell and the solvation structure of the electrolyte at low temperature. Reproduced from ref. 77. Copyright 2020, American Chemical Society. (d) *In situ* Raman installation diagram and spectra between the LFP cathode and PBF-FS-LPF_6. Reproduced from ref. 78. Copyright 2022, Wiley-VCH. (e) Schematic illustration of the evaluation of the SEI on MCMB in various electrolytes at −5 °C. Reproduced from ref. 79. Copyright 2019, Elsevier. (f) Schematic representation of the mechanism of the water scavenger to prevent DOL-based electrolyte gelation. Reproduced from ref. 80. Copyright 2023, Wiley-VCH.

the SEI. In the bilayer SEI, LiN_xO_y generated by ISDN dominates the top layer near the electrolyte, while LiF forms the bottom layer adjacent to the anode. The bilayer SEI improved the uniformity of Li deposition, reducing side reactions of active Li and electrolyte. Furthermore, Zhao *et al.*[77] incorporated $Cu(NO_3)_2$ into an ester-based electrolyte to regulate solvation behavior. The addition of $Cu(NO_3)_2$ suppressed the dissolution of transition metals and voltage decay, and improved the thermal stability of the cathode material.

3.3.2 F-containing additives to govern the transport of Li^+ ions. Fluoroethylene carbonate (FEC) is renowned for its film-forming capabilities and its ability to reduce on the anode surface before conventional carbonates, resulting in a denser solid electrolyte interphase (SEI). This property has led to its widespread use in enhancing interfacial stability. Thenuwara *et al.*[78] investigated the use of FEC-containing electrolytes for low-temperature battery applications (Fig. 7c). Compared to the DOL/DME electrolyte without additives, the addition of 10% FEC resulted in the formation of a stable, highly Li^+-conductive SEI. The FEC-modified electrolyte enabled cycling at temperatures as low as −60 °C with reasonable CE, which declined from 85% to 50% over 50 cycles. Notably, the SEI formed with the FEC-containing electrolyte was richer in inorganic species (LiF, Li_2CO_3) and thinner than that formed with the baseline electrolyte at both −20 °C and −40 °C. Additionally, several new fluorine-containing additives have been proposed. For instance, a commercial $LiPF_6$/EC/DMC electrolyte combined with 4,4′-sulfonyldiphenol (FS) and perfluoro *n*-butylsulfonyl fluoride (PBF) additives (referred to as PBF-FS-LPF_6) enabled lithium-metal batteries (LMBs) to operate at −40 °C. The fluorinated additive PBF altered the solvent sheath structure of the carbonate electrolyte and formed a fluorine-rich (LiF) SEI.[82] The emergence of highly electronegative sulfur (S) and FSI-derived S–N–S structures can be observed *via in situ* Raman spectroscopy (Fig. 7d), which effectively suppresses the decomposition of LiPF6 and thereby stabilizes the CEI.

3.3.3 S-containing additives to facilitate uniform Li deposition. Sulfur-containing additives can also function as film-forming agents, enhancing the stability and conductivity of the SEI.[83] Lan *et al.* demonstrated that the incorporation of *N-tert*-butyl-2-thiophenesulfonamide (NTSA) as a multifunctional electrolyte additive improved the electrochemical performance of $LiCoO_2$||ω-$Li_3V_2O_5$ full cells across a wide temperature range, primarily due to enhanced interfacial stability.[84] This performance enhancement was attributed to the decomposition of NTSA on the electrode surface, resulting in the formation of a uniform and robust electrode/electrolyte interphase. This interphase was enriched with multiple inorganic compounds, including LiF, Li_3N, and Li_2S, on both the cathode and anode surfaces. The inorganic-rich interface not only reduced the impedance of Li^+ migration at low temperatures but also improved the thermal stability of the interface, thereby enhancing the overall stability of the battery at both room and low temperatures. Another sulfur-containing additive, dimethyl sulfide (DMS), has also been employed to improve the low-temperature performance of electrolytes.[85]

3.3.4 P-containing additives to improve battery thermal stability. Phosphorus-containing additives are often recognized for their superior flame-retardant properties and can be employed to prevent thermal runaway caused by lithium plating or low-temperature preheating. Liao *et al.*[86] investigated the effect of lithium difluorobis(oxalato) phosphate (LiDFBOP) on electrochemical behavior at low temperatures. Their results showed that a graphite||NCM523 pouch cell with 1 wt% LiDFBOP maintained 93% of its initial capacity after 50 cycles at −20 °C and 0.5C, significantly outperforming the baseline electrolyte.[79] This performance was attributed to LiDFBOP's preferential oxidation on the cathode and reduction on the anode, forming a thin SEI rich in LiF, $Li_2C_2O_4$, and $Li_xPO_yF_z$, which ensured SEI stability and fast ionic conduction. Similarly, the addition of 1 wt% $LiPO_2F_2$ in the electrolyte resulted in 71.9% capacity retention at −20 °C in a graphite||NCM523 cell, compared to only 49.4% for cells with the baseline electrolyte.

Functional additives can also inhibit the high reactivity of esters with the anode. Xu *et al.*[80] explored the influences of (trimethylsilyl) phosphite (TMSP) and 1,3-propanediol cyclic sulfate (PCS) as additives in $LiPF_6^-$based electrolytes. This electrolyte expanded the electrochemical window of lithium-ion batteries (LIBs) to 3.5–5 V and enabled the batteries to function within a wide temperature range from −60 °C to 50 °C. Due to the lower lowest unoccupied molecular orbital (LUMO) of TMSP and PCS, they decompose prior to methyl acetate (MA) and carbonate solvents, generating an interface rich in P–O and $ROSO_2Li$, which suppresses the reaction of solvents and mesocarbon microbeads (MCMB). This facilitated the formation of a high-ionic-conductivity and stable SEI on the MCMB anode surface.

3.3.5 Other additives. Jiang *et al.*[87] proposed using an electrophile, trimethylsilyl isocyanate (SiNCO), as a water scavenger to inhibit the side reactions of 1,3-dioxolane (DOL), thus enabling DOL to remain liquid within a broad temperature range. SiNCO eliminates moisture by inhibiting the proton-induced ring-opening polymerization of the DOL electrolyte through a nucleophilic addition reaction. Analysis of the CEI revealed that the SiNCO additive contributed to the formation of a thin and inorganic-rich CEI.

Li *et al.* investigated the effect of cesium hexafluorophosphate ($CsPF_6$) as a film-forming additive in low-temperature electrolytes.[88] Cs^+ can enrich and promote the decomposition of ethylene carbonate (EC), forming a highly protective SEI, which in turn inhibits the decomposition of the propylene carbonate (PC) solvent and accelerates the migration of Li^+. Additionally, allyl sulfide (AS) has been identified as an electrolyte additive to reduce charge transfer resistance.[89] The incorporation of AS improved the discharge capacity of graphite electrodes, achieving capacities three times larger than those of cells with an electrolyte without AS at −30 °C.

3.4 Regulating the relationships among Li^+, solvent, and anions to manipulate solvation chemistry

Previous research has shown that the reduction in battery capacity and the increase in interface impedance at low temperatures are primarily due to sluggish desolvation, which constitutes the main kinetic barrier at the interface. Consequently, minimizing the desolvation energy barrier and optimizing the electrolyte solvent chemistry are key strategies for improving low-temperature battery performance.

3.4.1 Reduce solvent polarity to regulate the binding energy of the Li^+-solvent

Weakly solvated electrolytes (WSEs). Recently, weakly solvated electrolytes (WSEs) have emerged as a promising alternative for achieving solvated structures and properties similar to those of conventional systems, without the constraints of Li salt or diluent. WSEs contain solvents with weak solvating power, which are unable to fully dissociate lithium salts, leading to partial separation of cations and anions. This results in weaker interactions with Li^+ and allows more anions to coordinate with Li^+, forming abundant contact ion pairs (CIPs) and aggregates (AGGs).[90] Due to the strong coordination of Li^+ ions with anions rather than solvent molecules, the preferential formation of anion-derived inorganic SEI or CEI layers occurs when solvated Li^+ clusters are oxidized or reduced at the electrode/electrolyte interfaces. Examples of WSEs: (1) cyclopentylmethyl ether (CPME): a non-fluorinated ether solvent designed by Zhang *et al.*, which exhibits weak solvating power and remains liquid over a wide temperature range, enabling the tuning of solvating power and physicochemical properties (Fig. 8a).[91] (2) Bis(2-methoxyethoxy) methane (BME): developed by Wu *et al.*, this non-fluorinated

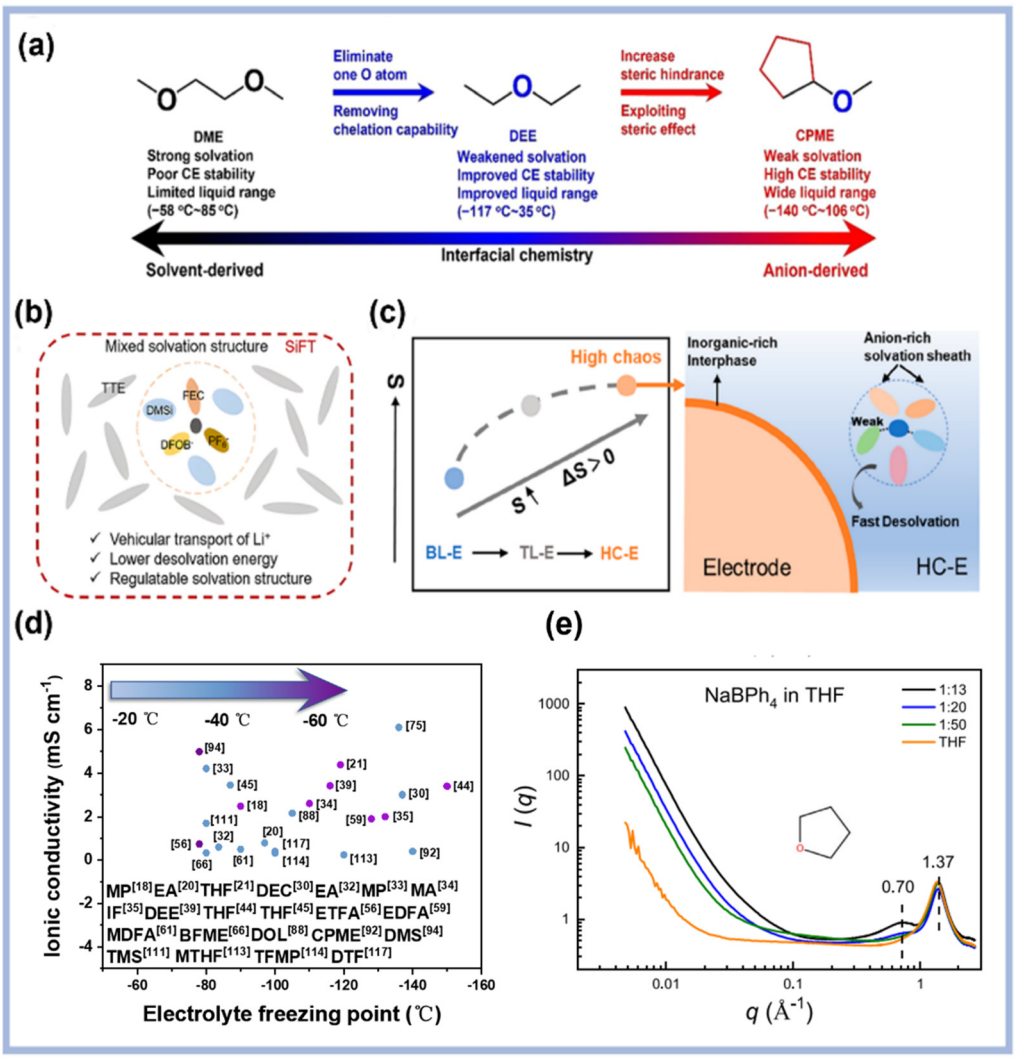

Fig. 8 (a) The solvation structure of the SiFT electrolyte. Reproduced from ref. 90. Copyright 2023, Elsevier. (b) Optimization mechanism of the high chaos electrolyte. Reproduced from ref. 93. Copyright 2023, American Chemical Society. (c) The binding energies between Li^+ and solvents/anions obtained by first-principles calculations. Reproduced from ref. 94. Copyright 2023, Wiley-VCH. (d) Summary of ionic conductivity at low temperatures and freezing points of popular electrolytes. (e) SAXS data of $NaBPh_4$ dissolved in THF with different salt concentrations. Reproduced from ref. 95. Copyright 2023, Springer Nature.

solvent uses a bi/tridentate coordination strategy to regulate solvation structures. BME has multiple oxygen sites that provide bi/tridentate chelation with Li^+ ions, forming an anion-rich Li^+ solvation shell.[92] Although WSEs exhibit lower desolvation energy, they suffer from reduced ionic conductivity and compromised reductive stability. Thus, incorporating co-solvents or additives becomes essential to balance ionic transport efficiency and interfacial stability.

Strongly solvated electrolytes with dual lithium salts. Zhao *et al.* proposed a strongly solvated electrolyte in dimethyl sulfite (DMS), which balances fast Li^+ conduction and efficient desolvation, resulting in a unique solvation structure.[93] LiFSI is highly dissociative in DMS, ensuring rapid Li^+ conduction. Additionally, the high affinity between difluoride (oxalate) borate anions (DFOB-) and Li^+ accelerates desolvation over a wide temperature range.

Limitations of WSEs. To address issues such as narrow electrochemical windows and poor ionic conductivity in electrolytes composed of weak solvents, the "strong-weak mixed solvent (HSWSS)" strategy has been proposed. This approach designs multi-component, hierarchically solvating electrolytes (HSE), such as the $LiPF_6$-LiDFOB-DMSI-FEC-TTE electrolyte, which expands the electrochemical window, improves ionic conductivity, and enhances dendrite suppression (Fig. 8b).[94]

Highly entropic electrolytes. Chen *et al.*[96] developed a highly entropic electrolyte rich in multiple anionic solvation structures that weakens Li^+ solvation, accelerates Li^+ desolvation at low temperatures, and improves charge transfer kinetics while inhibiting lithium dendrite growth (Fig. 8c). The electrolyte exhibits a self-adapting double-layer solvation structure, where free solvents weaken the binding energy between the Li^+–solvent and the Li^+–anion, while maintaining fast desolvation kinetics and low-temperature adaptability.[97,98] Using PTE312, full cells demonstrated outstanding capacities of 79% and 62.5% at −40 °C and −50 °C, respectively.

3.4.2 Low-concentration electrolytes (LCEs) to regulate lithium deposition behavior. Low-concentration electrolytes with low viscosity promote the formation of an anion-derived SEI and facilitate uniform lithium deposition on the lithium anode.[99,100] Wang *et al.* introduced an innovative ultralow-concentration electrolyte (ULCE). At −60 °C, the LMB with ULCE still exhibited a capacity of approximately 115 mA h g^{-1}, retaining about 57% of RTC.[101] However, the low lithium salt concentration in electrolytes reduces ionic conductivity, while excessive solvent content compromises stability and increases flammability. Addressing these challenges necessitates the use of non-solvating co-solvents or novel lithium salts to mitigate these limitations.

3.4.3 Highly concentrated electrolytes (HCEs) to form an anion-derived SEI. At high salt concentrations (typically 3–5 M), Li^+ ions coordinate with all solvent molecules and anions, creating a unique solution structure with negligible free solvent molecules. This structure contrasts sharply with conventional dilute solutions, which are dominated by free solvent molecules. In highly concentrated electrolytes (HCEs), the lowest unoccupied molecular orbital (LUMO) of the Li^+-solvation structure shifts from solvents to anions, resulting in an anion-derived SEI. Wang *et al.* developed a concentrated electrolyte that maintains stable charge–discharge cycling from −20 °C to 100 °C. The electrolyte's stable solvation structure and robust SEI contribute to its excellent electrochemical performance across a wide temperature range. At low temperatures, the highly Li^+-conductive SEI compensates for the electrolyte's reduced ionic conductivity, enabling stable cycling performance.[102] Although HCEs offer advantages such as high interfacial stability, a broad electrochemical window, and good compatibility, the high salt concentration in HCEs leads to challenges like increased viscosity, elevated freezing point, and poor wettability, which require further optimization.

3.4.4 Localized highly concentrated electrolytes (LHCEs) to balance Li^+–anion–solvent clusters. To address the challenges of high-concentration electrolytes (HCEs), researchers have introduced diluents to create localized high-concentration electrolytes (LHCEs).[103–105] The polarity mismatch between non-solvating diluents and solvating solvents drives the aggregation of free anions, lithium ions, and solvent molecules within the non-polar diluent.[106] This process maintains anion-participated solvation sheaths without increasing the lithium salt concentration.[107] Such a configuration promotes the formation of an inorganic-rich solid electrolyte interphase (SEI) through anion decomposition, thereby improving battery performance.[108] Chen *et al.* established design principles for LHCEs based on solvent properties.[109] These principles stipulate that the primary solvent should have a donor number (DN) >10, while the diluent should have a DN ≤10.

LHCEs can be conceptualized as droplets of a high-concentration electrolyte dispersed in an inert diluent, which neither dissolves lithium salt nor reacts with the solvent. The lithium salt concentration in each droplet exceeds 1 M and increases with the diluent proportion. Consequently, the selection of diluents and the regulation of their proportions are critical for LHCE performance.[110] Lin *et al.*[111] developed a multifunctional LHCE comprising a sulfolane (TMS)/ethyl acetate (EA)-based system, diluted with hydrofluoroether (HFE) and supplemented with a fluoroethylene carbonate (FEC) additive. A DMC/EC/TTE mixed electrolyte yielded a discharge capacity of 160.7 mA h g^{-1} at −30 °C.[112] Piao *et al.*[113] added tris(2,2,2-trifluoroethyl)orthoformate (TTE) to a mixed ether-based electrolyte (MixTHF) to decrease the donor oxygen's electronegativity in ether solvents, promoting anion participation in Li^+ solvation. Researchers have also explored ether fluorides as alternative diluents to fine-tune solvation structures and improve battery performance. Shi *et al.*[114] synthesized a novel amphiphilic solvent, 1,1,2,2-tetrafluoro-3-methoxypropane (TFMP), for use as an LHCE diluent. TFMP's lithiophilic segment efficiently solvates Li^+, facilitating the electrolyte's self-assembly into a unique core–shell solvation structure. Dichloromethane (DCM), another well-known diluent,[115] enabled the LHCEs to exhibit high ionic conductivity (0.6 mS cm^{-1}), low viscosity (0.35 Pa s), and enhanced oxidative stability at −70 °C. Fig. 8d summarizes the ionic conductivity at low temperatures and freezing points of representative electrolytes.

Fan *et al.*[116] used tetrafluoro-1-(2,2,2-trifluoroethoxy)ethane (D2) and methoxyperfluorobutane (M3) as diluents to modify all-fluorinated electrolytes' solvation structure, enhancing cell performance at low temperatures. Electrolytes comprising LiFSI-FEMC/FEC in D2 and LiBETI FEC/DEC–M3 exhibited enhanced ionic conductivity and lower desolvation energy. Cui *et al.* chose difluoromethane (DTF) as a co-solvent based on molecular electrostatic potential analysis.[117] DTF's moderate minimum electrostatic potential (−21.0 kcal mol^{-1}) balanced Li^+ affinity, preserving the anion-rich solvation structure. Additionally, the localized concentration strategy can also be applied to ionic liquid electrolytes. Liu *et al.* proposed a locally concentrated ionic liquid electrolyte ($[LiFSI]_1[EmimFSI]_2([dFBn]_2)$ named FEdF, 1,2-difluorobenzene (dFBn)), which enables Li||NCA cells to stably cycle 100 times at −20 °C at a 0.1C rate, achieving a capacity retention rate of 85.9%.[118] Although LHCEs can form highly stable interfaces with low viscosity and excellent wettability, challenges such as poor diluent compatibility, high cost, and environmental pollution issues still need to be resolved.

Table 1 A summary of recently reported low-temperature electrolytes for RLBs

Electrolyte formulation	Cathode/anode	Working temperature	Battery performance	Ref.
Salt engineering				
1 M $LiPF_6$ in MP : FEC (9 : 1, vol)	NCM111||graphite 2.7–4.3	−40 to RT	−20 °C@0.1C 92% after 100 cycles	18
2.4 M LiDFOB in EA/FEC	NCM9055||Li 2.8–4.3	−60 to RT	−40 °C@0.1C 100% after 100 cycles	22
$LiPF_6$: $LiBF_4$: LiDFOB (2 : 2 : 6, molar) in THF	NCM811||Li 2.7–4.3	−30 to RT	−30 °C@0.1C 93.4% after 100 cycles	123
1 M LiFSI in DMM	SPAN||Li 1.8–2.3	−40 to RT	−40 °C@0.1C 99.7% after 120 cycles	20
1 M $LiClO_4$ in ES/10%FEC	NCM811||Li 2.7–4.3	−50 to 70	−33 °C@0.1C 80% after 100 cycles	21
Solvent engineering				
Conventional solvents				
1 M $LiPF_6$ in EC : PC : DEC : EMC : EHFB (2 : 1 : 1.5 : 4 : 1.5, vol)	LCO||graphite 3.0–4.5	−100 to RT	−10 °C@0.1C 98% after 200 cycles	29
3 M $LiPF_6$ in EA : FEC (9 : 1, vol)	NLO||graphite 2.7–4.3	−40 to 60	−20 °C@0.2C 100% after 1400 cycles	33
1 M LiFSI in MP : FEC (9 : 1, vol)	LFP||graphite 2.5–4.2	−80 to 80	−40 °C@0.1C 67.7% after 100 cycles	34
1 M LiFSI in MA : FB (4 : 5, vol)	LCO||graphite 3.0–4.3	−60 to RT	−60 °C@0.05C 88.5% after 50 cycles	30
1 M LiDFOB in DMS/IF/FEC (35 : 45 : 20, vol)	LCO||Li 3.0–4.4	−70 to 60	−70 °C@1/15C 99% after 170 cycles	31
1 M LiFSI in DEE	SPAN||Li 1.8–2.3	−60 to RT	−40 °C@0.2C 60% after 50 cycles	38
1 M LiFSI in DOL/TTE 10 wt% FEC	NCM622||Li 3–4.3	−40 to RT	−40 °C@0.05C 76.1% after 15 cycles	44
0.5 M $LiPF_6$ 0.5 M LiFSI 0.1 M $LiNO_3$ in THF/FEC(9 : 1 vol)	NCM811||Li 2.7–4.3	−60 to RT	−30 °C@0.05C 78.6% after 50 cycles	42
1 M LiFSI in MTHF/THF (1 : 6, vol) 1 wt% $LiNO_3$	$CoSeO_x$ ||Li 1.4–3.5	−40 to RT	−40 °C@400 mAg^{-1} 84% after 100 cycles	43
Fluorinated solvents				
1.3 M LiFSI in FAN	Graphite ||Li 2.8–4.5	−80 to RT	−60 °C@0.2C 80% after 350 cycles	51
1 M $LiPF_6$ in MDFA/PFPN/FEC	NCM811||graphite 2.7–4.4	−50 to 60	−20 °C@0.2C 87.4% after 100 cycles	54
1 M LiFSI in ETFA	LTO||Li 1.8–2.8	−70 to RT	−40 °C@0.05C 99% after 50 cycles	56
1 M LiFSI in EDFA/FEC (9 : 1, vol)	NCM811||graphite 2.7–4.5	−40 to RT	−20 °C@0.2C 93% after 30 cycles	58
1 M $LiPF_6$ in DFEC/DEC (1 : 1, vol)	NCM811||Li 2.7–4.3	−30 to RT	−30 °C@0.2C 100% after 50 cycles	59
1 M LiFSI in MDFA/MDFSA/TTE	NCM811||graphite 2.7–4.5	−60 to 60	−30 °C@0.2C 82.8% after 350 cycles	60
1 M LiFSI in BFE	NCM811||Li 2.8–4.4	−60 to 60	−30 °C@1.75 mA cm^{-2} 90% after 150 cycles	64
1 M LiFSI in BFME	LFP||Graphite 2.7–4.3	−60 to 60	−20 °C@0.2C 92.5% after 200 cycles	65
Additive engineering				
1 M $LiPF_6$ in EC/EMC + FEC + $LiNO_3$ in TPPO	LFP||Li 2.5–4.0	−15 to 70	−15 °C@0.1C 100% after 100 cycles	71
1.6 M LiFSI in THF/MTHF (1 : 1 vol) with 2 wt% $LiNO_3$	LFP||Li 2.5–4.0	−40 to RT	−30 °C@0.1C 100% after 200 cycles	74
1 M $LiPF_6$ in EC/DMC (1 : 1 vol + 0.2% $LiNO_3$) + FS and PBF	LFP||Li 2.5–4.0	−40 to RT	−40 °C@0.5C 90% after 100 cycles	82
1 M $LiPF_6$ in EMC : DMC : FEC (4 : 4 : 2 vol) + 1%NTSA	$LiCoO_2$||ω-$Li_3V_2O_5$ 1.5–4.1	−30 to 80	−20 °C@0.2 A g^{-1} 100% after 100 cycles	84
2.5 M $LiBF_4$ in DOL/DME(7 : 3 vol) +Si-NCO	LCO||Li 3.0–4.2	−40 to RT	−40 °C@0.33C 80% after 150 cycles	87
1 M $LiPF_6$ in EC/EMC (1 : 2 vol) + 1% PhMS	NCM523||graphite 2.7–4.1	−10 to RT	−20 °C@0.1C 89% after 100 cycles	89
Solvation regulation				
LiFSI : CPME (1 : 10, molar)	LFP||Li 2.5–4.0	−20 to RT	−20 °C@0.2C 90% after 400 cycles	91
1 M LiFSI in BME	LFP||Li 2.5–4.0	−10 to 60	−10 °C@0.2C 86% after 100 cycles	92
0.6 M LiFSI 0.4 M LiDFOB in DMS	Graphite||Li 2.5–4.3	−78 to 60	−20 °C@0.1C −80% after 250 cycles	93
0.25 M LITFSI–0.75 M LIDFOB in TMS/EA/HFE FEC	NCM523||Li 3–4.6	−80 to 40	−40 °C@1C 97.5% after 200 cycles	111
1.5 M LiFSI in THF : MTHF/TTE	LFP||Li 2.5–4.0	−40 to RT	−40 °C@0.05C 100% after 150 cycles	113
1 M LiFSI in TFMP/DME(7 : 1, vol)	NCM811||Li 2.8–4.2	−40 to RT	−40 °C@0.2C 87% after 100 cycles	114
5 M LiFSI/EA + DCM (1 : 4, vol)	PI||Li 1.6–3.0	−70 to RT	−70 °C@0.2C 75% after 100 cycles	115
1 M LiFSI in EMC/FEC/DTF (1.5 : 1.5 : 7, vol)	NMC811||Li 2.7–4.8	−40 to RT	−40 °C@0.2C 93% after 100 cycles	117

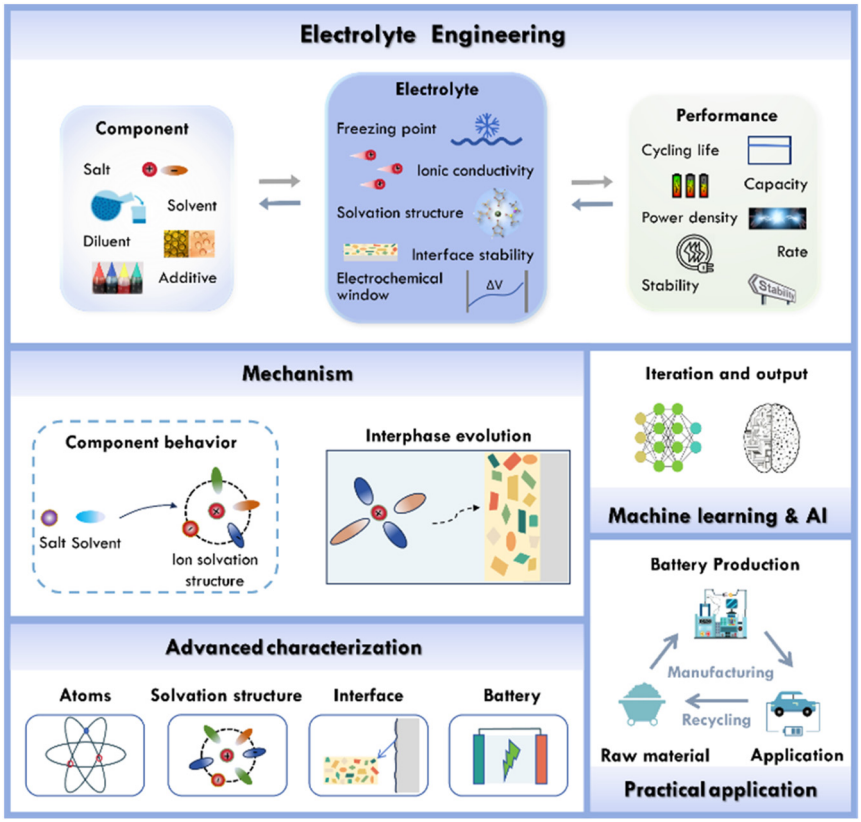

Fig. 9 The research and application opportunities for low-temperature electrolytes. Driven by several factors: (1) deeper insights into underlying mechanisms, (2) AI-assisted electrolyte design, (3) advanced characterization techniques, and (4) the need to balance environmental impact with battery performance are discussed.

3.4.5 Liquefied gas electrolyte to tune the viscosity at low temperatures. Meng *et al.*[119] introduced liquefied gas electrolytes (LGEs) as a novel type of wide-temperature-range stable electrolyte (WSE). LGEs utilize liquid hydrogen fluoride, primarily hydrofluorocarbons, as a solvent for salt dissolution. This results in an electrolyte with a wide electrochemical window (−3.23 to 2.47 V) over a broad temperature range. Liquid gases like fluoromethane exhibit significantly lower viscosity than conventional liquid electrolytes at ultra-low temperatures, enabling superior low-temperature electrochemical performance. The ionic conductivity of the fluoromethane (FM) solvent with 0.1 mol L^{-1} LiTFSI reaches 1.1 mS cm^{-1} at −60 °C, significantly surpassing conventional electrolytes. The addition of CO_2 as a film-forming additive to the original electrolyte results in a robust, Li-carbonate-rich SEI on the anode surface. Subsequent studies by Meng *et al.* incorporated acetonitrile and tetrahydrofuran (THF) as additive solvents, enhancing LiTFSI solubility in the FM-based electrolyte and reducing cell impedance.[120,121] Yin *et al.* designed a novel liquefied gas electrolyte (LGE) by incorporating liquefied dimethyl ether (Me_2O) into a mixture of 1,1,1,2-tetrafluoroethane (TFE) and pentafluoroethane (PFE).[122] This electrolyte maintains stable ionic conductivity (>1 mS cm^{-1}) across a wide temperature range (−78 °C to 80 °C) and enables Li/NMC622 batteries to achieve stable cycling over 200 cycles at −20 °C, with a capacity retention rate exceeding 90%. While these advancements significantly improved the low-temperature performance of lithium-metal batteries (LMBs), the tests were conducted under high-pressure conditions, and its practical application remains to be explored.

4. Conclusion and perspective

Traditional lithium batteries exhibit temperature-sensitive properties, which make it challenging to meet performance and cycle life requirements for devices operating at extreme temperatures. According to the Arrhenius equation, the electrochemical kinetics in rechargeable lithium batteries (RLBs) deteriorates as the temperature decreases. This slow kinetics leads to thermodynamic issues, such as lithium plating, which ultimately reduce battery performance. During the charging and discharging cycles of RLBs, charge transport, lithium-ion solvation and desolvation, and interfacial stability are all closely related to the electrolyte. As a result, the electrolyte plays a crucial role in determining the performance of RLBs at low temperatures. Traditional carbonate-based electrolytes exhibit a wide electrochemical window, but their viscosity

increases dramatically at low temperatures, rendering them unsuitable for extreme cold conditions (*e.g.*, below −20 °C). They are compatible with lithium-ion batteries, cost-effective, and supported by mature manufacturing processes. Ether-based electrolytes demonstrate low viscosity, good compatibility, and high ionic conductivity at low temperatures, functioning even below −40 °C. However, their poor oxidative stability limits their use with high-voltage cathodes like NMC811, although they are suitable for lithium-metal batteries. Liquefied gas electrolytes feature ultra-low viscosity and high ionic conductivity over a wide temperature range, making them ideal for broad-temperature lithium-metal batteries. However, they impose stringent sealing requirements on battery systems. In summary, conventional liquid electrolytes require optimized component design to reduce viscosity at low temperatures, enhance ionic conductivity, and broaden the electrochemical window, thereby improving battery performance in cold environments.

This review provides a comprehensive summary of the research progress on low-temperature electrolytes for lithium batteries, considering both the individual components and overall systems. Table 1 summarizes representative electrolytes and their battery low-temperature performance. Based on this foundation, we propose novel insights into potential solutions for improving the performance of low-temperature lithium batteries, as illustrated in Fig. 9.

4.1 Artificial intelligence and machine learning to optimize experiments

Capturing the intricate electrochemical processes in a battery using simple physical models is particularly challenging, especially at low temperatures. Furthermore, the physicochemical properties of the electrolyte, such as ionic conductivity and Li^+ migration number, can also impact the battery's performance, including capacity retention rate, cycle life, energy density, *etc*. Traditionally, most electrolytes have been designed through a trial-and-error approach, where accumulated experience is a key factor. This method, however, limits the development of new electrolytes and inhibits a deeper understanding of the redox mechanisms and solvation chemistry of electrolytes. Although methods based on dielectric constants and DN values have been proposed for selecting electrolyte components, they remain insufficiently comprehensive. Theoretical frameworks such as DFT and molecular dynamics (MD) have also been explored for electrolyte design, but their models are often too simplistic to accurately predict the specific components needed.

The integration of machine learning (ML) with prior material knowledge known as material knowledge-informed machine learning (MIML) holds significant potential for optimizing battery design. MIML compensates for traditional ML limitations, such as small sample sizes and poor interpretability.[124] For instance, deep learning algorithms have been used to improve the precision of numerical simulations, while neural networks have helped identify correlations between atomic polarizability and charge, which facilitates the prediction of molecular dynamics in liquid electrolytes. Additionally, the solvation environment of molecules can be simulated with neural networks, which enhances both the accuracy and speed of the predictive process.

MIML allows the introduction of prior theoretical models to reduce the amount of training data needed, resulting in more accurate outcomes. In recent years, with the use of big data and mechanisms, it is essential to observe the behavior of each component at varying spatial scales. Dave *et al.* developed Clio, a robotic platform that integrates robotics and machine learning (ML) to facilitate high-throughput experimentation and electrolyte property characterization for nonaqueous electrolytes.[125] Guided by experiment-planning algorithms, Clio autonomously optimizes the relationships between ionic conductivity, solvent mass fractions, and salt molality within defined design spaces. For example, Clio successfully optimized conductivity in a ternary solvent system consisting of ethylene carbonate (EC), ethyl methyl carbonate (EMC), and dimethyl carbonate (DMC) with $LiPF_6$ as the sole salt. This work illustrates the potential of autonomous robotics and integrated testing to accelerate the discovery of electrolytes for energy and materials science applications.

Techniques at the macroscale can offer an overview of the solvation process and identify fault locations, while nanoscale techniques can provide detailed insights into reaction mechanisms. For example, lithium dendrite formation in lithium metal batteries (LMBs) can be studied using optical microscopy, whereas TEM, with its smaller spatial scale, can monitor the progression of the SEI or CEI at specific locations.[126] Small-angle X-ray scattering (SAXS) can be employed to characterize nanostructures in electrolytes, enabling the analysis of molecular clusters, ion pairs, solvation sheaths of cations/anions, aggregates, and domain sizes of the electrolyte (Fig. 8e). Furthermore, when combined with molecular dynamics (MD) simulations, SAXS provides a powerful tool to investigate the working mechanisms of electrolytes.[95] The development of multi-scale characterization methods, addressing both temporal and spatial dimensions, will likely drive further advances in electrolyte design and improve battery performance.

4.2 Practical considerations for electrolytes

In practical research, it is essential to consider not only the impact of rechargeable low-temperature lithium battery electrolytes on battery performance but also their practical applications. For example, factors such as the influence of electrolyte quantity on energy density in pouch cells, the cost of new electrolytes, production feasibility, and the environmental impact must be taken into account. The potential of new electrolytes is closely linked to the overall battery system. In recent years, commercial sectors such as digital 3C electronics and new energy vehicles have driven the development of LIBs, leading to a reduction in manufacturing and material costs. However, compared to the widely used $LiPF_6$ electrolyte, the practical application of new electrolytes, such as HCEs (high-concentration electrolytes) and LHCEs (lithium-based high-

concentration electrolytes), is still constrained by the high cost of lithium salt types and diluents. $LiPF_6$, due to its cost-effectiveness and well-established production technology, is the most widely adopted lithium salt in commercial applications, with a current market price ranging from 20 to 30 US dollars per kilogram. However, $LiPF_6$ exhibits poor thermal stability and is susceptible to hydrolysis, leading to the formation of HF, which adversely affects the lifespan and safety performance of the electrolyte. In contrast, LiFSI, a novel sulfonimide-based lithium salt, demonstrates superior oxidation stability and low interfacial impedance. Nevertheless, constrained by factors such as complex synthesis processes, its cost remains significantly higher at 80 to 100 US dollars per kilogram, approximately 3 to 4 times that of $LiPF_6$, thus failing to meet large-scale market requirements. To facilitate widespread commercialization, it is imperative to develop continuous synthesis technologies or explore the use of blended lithium salts to effectively reduce costs. Despite their excellent wide-temperature performance and flame-retardant properties, fluorinated solvents may release hydrogen fluoride (HF) or fluorocarbons under high-temperature or abusive conditions, contributing to global warming. These compounds are difficult to degrade *via* conventional treatment methods. Before commercialization, it is essential to enhance recycling technologies, conduct thorough environmental risk assessments, and develop low-global-warming-potential (GWP) alternatives to mitigate ecological impacts.

In current research on low-temperature electrolytes, researchers often conduct low-temperature battery testing using small-capacity coin cells, while there are relatively few reports on low-temperature long-cycle testing of high-capacity batteries, such as pouch cells. The stainless-steel casing of coin cells allows them to withstand pressure from gas accumulation during charge–discharge cycles caused by electrode changes and electrolyte consumption. However, due to the material properties of their gaskets, coin cells exhibit higher internal resistance, making them prone to side reactions during cycling, which results in lower capacity retention.

In contrast, pouch cells feature a simpler structure, lower internal resistance, and superior rate performance. Yet, their large surface area and soft aluminum–plastic film outer layer make them susceptible to gas-induced swelling, generating harmful additional stresses that can lead to battery failure. The compact size and limited capacity of coin cells mask deficiencies in electrolyte properties, such as the film-forming capability. Furthermore, the electrolyte-to-capacity (E/C) ratios differ significantly between coin and pouch cells, with the latter being substantially lower.[127] Therefore, to enhance battery capacity and expand device applications, there is an urgent need for low-temperature electrolytes with improved film-forming ability and electrochemical stability.

4.3 Non-traditional systems for low-temperature batteries

While improvements in electrolytes can enhance the low-temperature performance of lithium batteries to some extent, many modification strategies have not yet been practical for widespread application. Alternative solutions can be found at the operational level. During battery charging and discharging at low temperatures, high resistance leads to the conversion of a significant amount of electrical energy into heat. This heat generated by the charging and discharging process, can be utilized for warming the interior of the battery. This process can be facilitated through Battery Management Systems (BMS) in various ways, allowing the battery to regain performance once its temperature rises above zero degrees Celsius.[128]

A novel approach that has emerged in recent years is the self-heating battery. In this system, the battery generates heat solely through its internal resistance (*i.e.*, ohmic and polarization resistance). For a single battery, adjusting the discharge current is sufficient to initiate self-heating. Theoretically, self-heating technology can heat the battery faster and more uniformly, offering additional advantages in terms of energy consumption, temperature uniformity, cost, and minimal weight increase.

Data availability

No data were used for the research described in the article.

Conflicts of interest

The authors declare that they have no known competing financial interests or personal relationships that could have appeared to influence the work reported in this paper.

Acknowledgements

This work was supported by the Anhui Provincial Natural Science Foundation (2208085Y05), the Anhui Provincial Scientific Reuter Foundation for Returned Scholars (2022LCX030), the Excellent Research and Innovation Team Project of Anhui Province (2022AH010001), the National Natural Science Foundation of China (52172173) and Guangxi Key Laboratory of Low Carbon Energy Material (2021GXKLLCEM04). N. Wang acknowledges the support from the Australia Research Council (DP240102926 and FT240100596).

References

1 Z. Yu, P. E. Rudnicki, Z. Zhang, Z. Huang, H. Celik, S. T. Oyakhire, Y. Chen, X. Kong, S. C. Kim, X. Xiao, H. Wang, Y. Zheng, G. A. Kamat, M. S. Kim, S. F. Bent, J. Qin, Y. Cui and Z. Bao, *Nat. Energy*, 2022, **7**, 94–106.
2 Z. Li, Y. Yao, S. Sun, C. Jin, N. Yao, C. Yan and Q. Zhang, *Angew. Chem.*, 2023, **135**, e202303888.
3 S. Zhang, Q. Fan, C. Zhang, T. Zhou, K. Kalantar-Zadeh and Z. Guo, *Energy Environ. Sci.*, 2021, **14**, 4177–4202.

4 E. Fan, L. Li, Z. Wang, J. Lin, Y. Huang, Y. Yao, R. Chen and F. Wu, *Chem. Rev.*, 2020, **120**, 7020–7063.
5 X. Zhou, Y. Zhou, L. Yu, L. Qi, K. S. Oh, P. Hu, S. Y. Lee and C. Chen, *Chem. Soc. Rev.*, 2024, **53**, 5291–5337.
6 D. Hubble, D. E. Brown, Y. Zhao, C. Fang, J. Lau, B. D. McCloskey and G. Liu, *Energy Environ. Sci.*, 2022, **15**, 550.
7 N. Zhang, T. Deng, S. Zhang, C. Wang, L. Chen, C. Wang and X. Fan, *Adv. Mater.*, 2022, **34**, 2107899.
8 A. Hu, F. Li, W. Chen, T. Lei, Y. Li, Y. Fan, M. He, F. Wang, M. Zhou, Y. Hu, Y. Yan, B. Chen, J. Zhu, J. Long, X. Wang and J. Xiong, *Adv. Energy Mater.*, 2022, **12**, 2202432.
9 W. Bai, J. Gao, K. Li, G. Wang, T. Zhou, P. Li, S. Qin, G. Zhang, Z. Guo, C. Xiao and Y. Xie, *Angew. Chem.*, 2020, **132**, 17647–17651.
10 D. Hubble, D. E. Brown, Y. Zhao, C. Fang, J. Lau, B. D. McCloskey and G. Liu, *Energy Environ. Sci.*, 2022, **15**, 550–578.
11 Y. Tang, Y. Zhang, W. Li, B. Ma and X. Chen, *Chem. Soc. Rev.*, 2015, **44**, 5926–5940.
12 Q. Liu and L. Wang, *Adv. Energy Mater.*, 2023, **13**, 2301742.
13 Y. Sun, B. Liu, L. Liu and X. Yan, *Adv. Funct. Mater.*, 2022, **32**, 2109568.
14 Z. Piao, R. Gao, Y. Liu, G. Zhou and H. Cheng, *Adv. Mater.*, 2022, **35**, 2206009.
15 Y. Feng, L. Zhou, H. Ma, Z. Wu, Q. Zhao, H. Li, K. Zhang and J. Chen, *Energy Environ. Sci.*, 2022, **15**, 1711–1759.
16 K. Yang, R. Tian, Z. Wang, H. Zhang, Y. Ma, X. Shi, D. Song, L. Zhang and L. Z, *Rare Met.*, 2023, **42**, 4128–4141.
17 J. Hou, M. Yang, D. Wang and J. Zhang, *Adv. Energy Mater.*, 2020, **10**, 1904152.
18 Y. Cho, M. Li, J. Holoubek, W. Li, Y. Yin, Y. S. Meng and Z. Chen, *ACS Energy Lett.*, 2021, **6**, 2016–2023.
19 S. Zhang, *Electrochem. Commun.*, 2006, **8**, 1423–1428.
20 T. Ma, Y. Ni, Q. Wang, W. Zhang, S. Jin, S. Zheng, X. Yang, Y. Hou, Z. Tao and J. Chen, *Angew. Chem., Int. Ed.*, 2022, **61**, e202207927.
21 Y. Wang, Z. Li, W. Xie, Q. Zhang, Z. Hao, C. Zheng, J. Hou, Y. Lu, Z. Yan, Q. Zhao and J. Chen, *Angew. Chem.*, 2024, **136**, e202310905.
22 R. Han, Z. Wang, D. Huang, F. Zhang, A. Pan, H. Song, Y. Wei, Y. Liu, L. Wang, Y. Liu, J. Xu and X. Wu, *Small*, 2023, **19**, 2300571.
23 C. Jin, N. Yao, Y. Xiao, J. Xie, Z. Li, X. Chen, B. Li, X. Zhang, J. Huang and Q. Zhang, *Adv. Mater.*, 2022, **35**, 2208340.
24 L. Xiao, Y. Cao, X. Ai and H. Yang, *Electrochim. Acta*, 2004, **49**, 4857–4863.
25 H. Li, R. Hua, Y. Xu, D. Ke, C. Yang, Q. Ma, L. Zhang, T. Zhou and C. Zhang, *Chem. Sci.*, 2023, **14**, 10147–10154.
26 S. Zhang, Y. Zheng, X. Huang, J. Hong, B. Cao, J. Hao, Q. Fan, T. Zhou and Z. Guo, *Adv. Energy Mater.*, 2019, **9**, 1900081.
27 M. C. Smart, B. V. Ratnakumar, K. B. Chin and L. D. Whitcanack, *J. Electrochem. Soc.*, 2010, **157**, A1361.
28 K. Chen, Z. Yu, S. Deng, Q. Wu, J. Zou and X. Zeng, *J. Power Sources*, 2015, **278**, 411–419.
29 Y. Chen, Q. He, Y. Zhao, W. Zhou, P. Xiao, P. Gao, N. Tavajohi, J. Tu, B. Li, X. He, L. Xing, X. Fan and J. Liu, *Nat. Commun.*, 2023, **14**, 8326.
30 S. Lei, Z. Zeng, H. Yan, M. Qin, M. Liu, Y. Wu, H. Zhang, S. Cheng and J. Xie, *Adv. Funct. Mater.*, 2023, **33**, 2301028.
31 J. Liu, B. Yuan, N. He, L. Dong, D. Chen, S. Zhong, Y. Ji, J. Han, C. Yang, Y. Liu and W. He, *Energy Environ. Sci.*, 2023, **16**, 1024–1034.
32 L. Tan, P. Chen, Q. Chen, X. Huang, K. Zou, Y. Nie and L. Li, *Rare Met.*, 2023, **42**, 4081–4090.
33 Z. Li, N. Yao, L. Yu, Y. Yao, C. Jin, Y. Yang, Y. Xiao, X. Yue, W. Cai, L. Xu, P. Wu, C. Yan and Q. Zhang, *Matter*, 2023, **6**, 2274–2292.
34 Z. Li, Y. Yao, M. Zheng, S. Sun, Y. Yang, Y. Xiao, L. Xu, C. Jin, X. Yue, T. Song, P. Wu, C. Yan and Q. Zhang, *Angew. Chem.*, 2024, **137**, e202409409.
35 X. Dai, K. Zou, W. Jing, P. Xu, J. Sun, S. Guo, Q. Tan, Y. Liu, T. Zhou and Y. Chen, *J. Mater. Chem. A*, 2022, **10**, 16152–16162.
36 K. Yang, R. Tian, Z. Wang, H. Zhang, Y. Ma, X. Shi, D. Song, L. Zhang and L. Zhu, *Rare Met.*, 2023, **42**, 4128–4141.
37 Q. Fan, J. Jiang, S. Zhang, T. Zhou, W. K. Pang, Q. Gu, H. Liu, Z. Guo and J. Wang, *Adv. Energy Mater.*, 2021, **11**, 2100957.
38 J. Holoubek, H. Liu, Z. Wu, Y. Yin, X. Xing, G. Cai, S. Yu, H. Zhou, T. A. Pascal, Z. Chen and P. Liu, *Nat. Energy*, 2021, **6**, 303–313.
39 R. Xu, S. Zhang, X. Shen, N. Yao, J. Ding, Y. Xiao, L. Xu, C. Yan and J. Huang, *Small Struct.*, 2023, **4**, 2200400.
40 G. Cai, J. Holoubek, M. Li, H. Gao, Y. Yin, S. Yu, H. Liu, T. A. Pascal, P. Liu and Z. Chen, *Proc. Natl. Acad. Sci. U. S. A.*, 2022, **119**, e2200392119.
41 S. Chen, J. Fan, Z. Cui, L. Tan, D. Ruan, X. Zhao, J. Jiang, S. Jiao and X. Ren, *Angew. Chem., Int. Ed.*, 2023, **62**, e202219310.
42 P. Liang, H. Hu, Y. Dong, Z. Wang, K. Liu, G. Ding and F. Cheng, *Adv. Funct. Mater.*, 2024, **34**, 2309858.
43 L. Cheng, Y. Wang, J. Yang, M. Tang, C. Zhang, Q. Zhu, S. Wang, Y. Li, P. Hu and H. Wang, *Adv. Funct. Mater.*, 2022, **33**, 2212349.
44 S. G. Yoon, K. A. Cavallaro, B. J. Park, H. Yook, J. W. Han and M. T. McDowell, *Adv. Funct. Mater.*, 2023, **33**, 2302778.
45 K. Naoi, E. Iwama, N. Ogihara, Y. Nakamura, H. Segawa and Y. Ino, *J. Electrochem. Soc.*, 2009, **156**, A272.
46 Z. Liu, R. Wang, Q. Ma, H. Kang, L. Zhang, T. Zhou and C. Zhang, *Carbon Neutralization*, 2022, **1**, 126–139.
47 J. Cuan, Y. Zhou, T. Zhou, S. Ling, K. Rui, Z. Guo, H. Liu and X. Yu, *Adv. Mater.*, 2019, **31**, 1803533.
48 M. Jiang, F. Zhang, G. Zhu, Y. Ma, W. Luo, T. Zhou and J. Yang, *ACS Appl. Mater. Interfaces*, 2020, **12**, 24796–24805.
49 L. Luo, K. Chen, H. Chen, H. Li, R. Cao, X. Feng, W. Chen, Y. Fang and Y. Cao, *Adv. Mater.*, 2023, **36**, 2308881.

50 T. Zheng, J. Xiong, B. Zhu, X. Shi, Y.-J. Cheng, H. Zhao and Y. Xia, *J. Mater. Chem. A*, 2021, **9**, 9307–9318.
51 D. Lu, R. Li, M. M. Rahman, P. Yu, L. Lv, S. Yang, Y. Huang, C. Sun, S. Zhang, H. Zhang, J. Zhang, X. Xiao, T. Deng, L. Fan, L. Chen, J. Wang, E. Hu, C. Wang and X. Fan, *Nature*, 2024, **627**, 101–107.
52 N. Von Aspern, G.-V. Röschenthaler, M. Winter and I. Cekic-Laskovic, *Angew. Chem., Int. Ed.*, 2019, **58**, 15978–16000.
53 H. Li, R. Hua, Y. Xu, D. Ke, C. Yang, Q. Ma, L. Zhang, T. Zhou and C. Zhang, *Chem. Sci.*, 2023, **14**, 10147–10154.
54 Y. Zou, Z. Ma, G. Liu, Q. Li, D. Yin, X. Shi, Z. Cao, Z. Tian, H. Kim, Y. Guo, C. Sun, L. Cavallo, L. Wang, H. N. Alshareef, Y. Sun and J. Ming, *Angew. Chem.*, 2023, **135**, e202216189.
55 Y. Yang, Z. Fang, Y. Yin, Y. Cao, Y. Wang, X. Dong and Y. Xia, *Angew. Chem., Int. Ed.*, 2022, **61**, e202208345.
56 Y. Yang, P. Li, N. Wang, Z. Fang, C. Wang, X. Dong and Y. Xia, *Chem. Commun.*, 2020, **56**, 9640–9643.
57 Z. Cui, C. Liu and A. Manthiram, *Adv. Mater.*, 2024, **36**, 2409272.
58 Y. Mo, G. Liu, Y. Yin, M. Tao, J. Chen, Y. Peng, Y. Wang, Y. Yang, C. Wang, X. Dong and Y. Xia, *Adv. Energy Mater.*, 2023, **13**, 2301285.
59 Z. Wang, Z. Sun, Y. Shi, F. Qi, X. Gao, H. Yang, H.-M. Cheng and F. Li, *Adv. Energy Mater.*, 2021, **11**, 2100935.
60 J. Xu, J. Zhang, T. P. Pollard, Q. Li, S. Tan, S. Hou, H. Wan, F. Chen, H. He, E. Hu, K. Xu, X. Yang, O. Borodin and C. Wang, *Nature*, 2023, **614**, 694–700.
61 P. Xiao, Y. Zhao, Z. Piao, B. Li, G. Zhou and H. Cheng, *Energy Environ. Sci.*, 2022, **15**, 2435–2444.
62 R. Wang, H. Wang, H. Zhao, M. Yuan, Z. Liu, G. Zhang, T. Zhang, Y. Qian, J. Wang, I. Lynch and Y. Deng, *Energy Mater.*, 2023, **3**, 300040.
63 Y. Yang, W. Yang, H. Yang and H. Zhou, *eScience*, 2023, **3**, 100170.
64 G. Zhang, J. Chang, L. Wang, J. Li, C. Wang, R. Wang, G. Shi, K. Yu, W. Huang, H. Zheng, T. Wu, Y. Deng and J. Lu, *Nat. Commun.*, 2023, **14**, 1081.
65 Y. Xue, Y. Wang, H. Zhang, W. Kong, Y. Zhou, B. Kang, Z. Huang and H. Xiang, *Angew. Chem., Int. Ed.*, 2024, **137**, e202414201.
66 L. Tan, P. Chen, Q. Chen, X. Huang, K. Zou, Y. Nie and L. Li, *Rare Met.*, 2023, **42**, 4081–4090.
67 L. Jiang, C. Yan, Y. Yao, W. Cai, J. Huang and Q. Zhang, *Angew. Chem., Int. Ed.*, 2021, **60**, 3402–3406.
68 X. Zhang, X. Chen, X. Cheng, B. Li, X. Shen, C. Yan, J. Huang and Q. Zhang, *Angew. Chem., Int. Ed.*, 2018, **57**, 5301–5305.
69 N. Xin, Y. Sun, M. He, C. J. Radke and J. M. Prausnitz, *Fluid Phase Equilib.*, 2018, **461**, 1–7.
70 X. Xu, X. Yue, Y. Chen and Z. Liang, *Angew. Chem., Int. Ed.*, 2023, **62**, e202306963.
71 P. Xiao, R. Luo, Z. Piao, C. Li, J. Wang, K. Yu, G. Zhou and H. M. Cheng, *ACS Energy Lett.*, 2021, **6**, 3170–3179.
72 H. Chen, K. Chen, L. Luo, X. Liu, Z. Wang, A. Zhao, H. Li, X. Ai, Y. Fang and Y. Cao, *Angew. Chem., Int. Ed.*, 2024, **63**, e202316966.
73 Z. Jiang, T. Yang, C. Li, J. Zou, H. Yang, Q. Zhang and Y. Li, *Adv. Funct. Mater.*, 2023, **33**, 2306868.
74 R. Yu, Z. Li, X. Zhang and X. Guo, *Chem. Commun.*, 2022, **58**, 8994–8997.
75 F. Qiu, X. Li, H. Deng, D. Wang, X. Mu, P. He and H. Zhou, *Adv. Energy Mater.*, 2019, **9**, 1803372.
76 N. Piao, S. Liu, B. Zhang, X. Ji, X. Fan, L. Wang, P. Wang, T. Jin, S. Liou, H. Yang, J. Jiang, K. Xu, M. A. Schroeder, X. He and C. Wang, *ACS Energy Lett.*, 2021, **6**, 1839–1848.
77 R. Zhao, X. Li, Y. Si, W. Guo and Y. Fu, *ACS Appl. Mater. Interfaces*, 2021, **13**, 40582–40589.
78 A. C. Thenuwara, P. P. Shetty, N. Kondekar, S. E. Sandoval, K. Cavallaro, R. May, C. Yang, L. E. Marbella, Y. Qi and M. T. McDowell, *ACS Energy Lett.*, 2020, **5**, 2411–2420.
79 B. Yang, H. Zhang, L. Yu, W. Fan and D. Huang, *Electrochim. Acta*, 2016, **221**, 107–114.
80 G. Xu, S. Huang, Z. Cui, X. Du, X. Wang, D. Lu, X. Shangguan, J. Ma, P. Han, X. Zhou and G. Cui, *J. Power Sources*, 2019, **416**, 29–36.
81 Q. Zhang, S. Sun, M. Zhou, L. Hou, J. Liang, S. Yang, B. Li, X. Zhang and J. Huang, *Angew. Chem.*, 2023, **135**, e202306889.
82 D. Zhang, D. Zhu, W. Guo, C. Deng, Q. Xu, H. Li and Y. Min, *Adv. Funct. Mater.*, 2022, **32**, 2112764.
83 J. Chen, Y. Zhang, H. Lu, J. Ding, X. Wang, Y. Huang, H. Ma and J. Wang, *eScience*, 2023, **3**, 100135.
84 X. Lan, S. Yang, T. Meng, C. Zhang and X. Hu, *Adv. Energy Mater.*, 2023, **13**, 2203449.
85 G. Kang, G. Zhong, K. Cai, J. Ma, J. Biao, Y. Cao, S. Lu, K. Yu, F. Kang and Y. Cao, *ACS Energy Lett.*, 2024, **9**, 2572–2581.
86 B. Liao, H. Li, M. Xu, L. Xing, Y. Liao, X. Ren, W. Fan, L. Yu, K. Xu and W. Li, *Adv. Energy Mater.*, 2018, **8**, 1800802.
87 H. Jiang, C. Yang, M. Chen, X. Liu, L. Yin, Y. You and J. Lu, *Angew. Chem., Int. Ed.*, 2023, **62**, e202300238.
88 Y. Lin, X. Yue, H. Zhang, L. Yu, W. Fan and T. Xie, *Electrochim. Acta*, 2019, **300**, 202–207.
89 S. Jurng, S. Park, T. Yoon, H. Kim, H. Jeong, J. H. Ryu, J. J. Kim and S. M. Oh, *J. Electrochem. Soc.*, 2016, **163**, A1798–A1804.
90 Y. Yao, X. Chen, C. Yan, X. Zhang, W. Cai, J. Huang and Q. Zhang, *Angew. Chem., Int. Ed.*, 2021, **60**, 4090–4097.
91 H. Zhang, Z. Zeng, F. Ma, Q. Wu, X. Wang, S. Cheng and J. Xie, *Angew. Chem.*, 2023, **135**, e202300771.
92 J. Wu, Z. Gao, Y. Tian, Y. Zhao, Y. Lin, K. Wang, H. Guo, Y. Pan, X. Wang, F. Kang, N. Tavajohi, X. Fan and B. Li, *Adv. Mater.*, 2023, **35**, 2303347.
93 Y. Zhao, Z. Hu, Z. Zhao, X. Chen, S. Zhang, J. Gao and J. Luo, *J. Am. Chem. Soc.*, 2023, **145**, 22184–22193.
94 J. Wu, S. Zhang, C. Yang, X. Zhang, M. Zhou, W. Liu and H. Zhou, *Energy Storage Mater.*, 2023, **63**, 103043.
95 K. Qian, Z. Yu, Y. Liu, D. Gosztola, R. Winans, L. Cheng and T. Li, *J. Energy Chem.*, 2022, **70**, 340–346.
96 F. Cheng, W. Zhang, Q. Li, C. Fang, J. Han and Y. Huang, *ACS Nano*, 2023, **17**, 24259–24267.

97 L. Chen, J. Wang, M. Chen, Z. Pan, Y. Ding, Z. Song, X. Ai, Y. Cao and Z. Chen, *Energy Storage Mater.*, 2024, **65**, 103098.
98 Q. Ma, J. Zheng, H. Kang, L. Zhang, Q. Zhang, H. Li, R. Wang, T. Zhou, Q. Chen, A. Liu, H. Li and C. Zhang, *ACS Appl. Mater. Interfaces*, 2021, **13**, 43002–43010.
99 L. Liu, Z. Shadike, N. Wang, Y. Chen, X. Cai, E. Hu and J. Zhang, *eScience*, 2024, **3**, 100268.
100 L. Liu, Z. Shadike, N. Wang, Y. Chen, X. Cai, E. Hu and J. Zhang, *eScience*, 2024, **4**, 100268.
101 Z. Wang, H. Zhang, J. Xu, A. Pan, F. Zhang, L. Wang, R. Han, J. Hu, M. Liu and X. Wu, *Adv. Funct. Mater.*, 2022, **32**, 2112598.
102 J. Wang, Q. Zheng, M. Fang, S. Ko, Y. Yamada and A. Yamada, *Adv. Sci.*, 2021, **8**, 2101646.
103 X. Cao, H. Jia, W. Xu and J.-G. Zhang, *J. Electrochem. Soc.*, 2021, **168**, 010522.
104 J. Cuan, Y. Zhou, T. Zhou, S. Ling, K. Rui, Z. Guo, H. Liu and X. Yu, *Adv. Mater.*, 2019, **31**, 1803533.
105 H. Wu, X. Zhou, C. Yang, D. Xu, Y.-H. Zhu, T. Zhou, S. Xin and Y. You, *ACS Appl. Mater. Interfaces*, 2023, **15**, 18828–18835.
106 H. Jia, J. Kim, P. Gao, Y. Xu, M. H. Engelhard, B. E. Matthews, C. Wang and W. Xu, *Angew. Chem.*, 2023, **135**, e202218005.
107 H. Wang, J. Liu, J. He, S. Qi, M. Wu, F. Li, J. Huang, Y. Huang and J. Ma, *eScience*, 2022, **2**, 557–565.
108 J. Duan, H. Pei, Q. Yang, X. Li, X. Ba, X. Yong, J. Guo and S. Lu, *Rare Met.*, 2024, **43**, 2560–2573.
109 J. Chen, H. Zhang, M. Fang, C. Ke, S. Liu and J. Wang, *ACS Energy Lett.*, 2023, **8**, 1723–1734.
110 J. Holoubek, K. Kim, Y. Yin, Z. Wu, H. Liu, M. Li, A. Chen, H. Gao, G. Cai, T. A. Pascal, P. Liu and Z. Chen, *Energy Environ. Sci.*, 2022, **15**, 1647–1658.
111 S. Lin, H. Hua, P. Lai and J. Zhao, *Adv. Energy Mater.*, 2021, **11**, 2101775.
112 X. Zhang, L. Zou, Y. Xu, X. Cao, M. H. Engelhard, B. E. Matthews, L. Zhong, H. Wu, H. Jia, X. Ren, P. Gao, Z. Chen, Y. Qin, C. Kompella, B. W. Arey, J. Li, D. Wang, C. Wang, J. Zhang and W. Xu, *Adv. Energy Mater.*, 2020, **10**, 2000368.
113 N. Piao, J. Wang, X. Gao, R. Li, H. Zhang, G. Hu, Z. Sun, X. Fan, H. Cheng and F. Li, *J. Am. Chem. Soc.*, 2024, **146**, 18281–18291.
114 J. Shi, C. Xu, J. Lai, Z. Li, Y. Zhang, Y. Liu, K. Ding, Y. Cai, R. Shang and Q. Zheng, *Angew. Chem.*, 2023, **135**, e202218151.
115 X. Dong, Y. Lin, P. Li, Y. Ma, J. Huang, D. Bin, Y. Wang, Y. Qi and Y. Xia, *Angew. Chem., Int. Ed.*, 2019, **58**, 5623–5627.
116 X. Fan, X. Ji, L. Chen, J. Chen, T. Deng, F. Han, J. Yue, N. Piao, R. Wang, X. Zhou, X. Xiao, L. Chen and C. Wang, *Nat. Energy*, 2019, **4**, 882–890.
117 Z. Cui, D. Wang, J. Guo, Q. Nian, D. Ruan, J. Fan, J. Ma, L. Li, Q. Dong, X. Luo, Z. Wang, X. Ou, R. Cao, S. Jiao and X. Ren, *J. Am. Chem. Soc.*, 2024, **146**, 27644–27654.
118 X. Liu, A. Mariani, T. Diemant, X. Dong, P. Su and S. Passerini, *Angew. Chem., Int. Ed.*, 2023, **62**, e202305840.
119 C. S. Rustomji, Y. Yang, T. K. Kim, J. Mac, Y. J. Kim, E. Caldwell, H. Chung and S. Meng, *Science*, 2017, **356**, eaal4263.
120 Y. Y. C. Yang, D. M. Davies, Y. J. Yin, O. Borodin, J. Z. Lee, C. C. Fang, M. Olguin, Y. H. Zhang, E. S. Sablina, X. F. Wang, C. S. Rustomji and Y. S. Meng, *Joule*, 2019, **3**, 1986–2000.
121 Y. Yang, Y. Yin, D. M. Davies, M. Zhang, M. Mayer, Y. Zhang, E. S. Sablina, S. Wang, J. Z. Lee, O. Borodin, C. S. Rustomji and Y. S. Meng, *Energy Environ. Sci.*, 2020, **13**, 2209–2219.
122 Y. Yin, Y. Yang, D. Cheng, M. Mayer, J. Holoubek, W. Li, G. Raghavendran, A. Liu, B. Lu, D. D. Z. Chen, O. Borodin and Y. Meng, *Nat. Energy*, 2022, **7**, 548–559.
123 P. Liang, J. Li, Y. Dong, Z. Wang, G. Ding, K. Liu, L. Xue and F. Cheng, *Angew. Chem., Int. Ed.*, 2024, **03**, e202415853.
124 Z. Li, Y. Yao, M. Zheng, S. Sun, Y. Yang, Y. Xiao, L. Xu, C. Jin, X. Yue, T. Song, P. Wu, C. Yan and Q. Zhang, *Angew. Chem., Int. Ed.*, 2024, **137**, e202409409.
125 A. Dave, J. Mitchell, S. Burke, H. Lin, J. Whitacre and V. Viswanathan, *Nat. Commun.*, 2022, **13**, 5454.
126 E. Miele, W. M. Dose, I. Manyakin, M. H. Frosz, Z. Ruff, M. F. L. De Volder, C. P. Grey, J. J. Baumberg and T. G. Euser, *Nat. Commun.*, 2022, **13**, 1651.
127 X. Zhou, Y. Zhou, L. Yu, L. Qi, K.-S. Oh, P. Hu, S.-Y. Lee and C. Chen, *Chem. Soc. Rev.*, 2024, **53**, 5291–5337.
128 X. Hu, Y. Zheng, D. A. Howey, H. Perez, A. Foley and M. Pecht, *Prog. Energy Combust. Sci.*, 2020, **77**, 100806.